The nuclear matrix protein CIZ1 facilitates localisation of Xist RNA to the inactive X-chromosome territory

Rebeca Ridings-Figueroa[1]*, Emma R Stewart[1], Tatyana B Nesterova[2], Heather Coker[2], Greta Pintacuda[2], Jonathan Godwin[2], Rose Wilson[1]**, Aidan Haslam[1], Fred Lilley[1], Renate Ruigrok[3], Sumia A Bageghni[3], Ghadeer Albadrani[3], William Mansfield[4], Jo-An Roulson[5], Neil Brockdorff[2], Justin FX Ainscough[3,1] Dawn Coverley[1]

[1] Department of Biology, University of York, YO10 5DD, UK

[2] Department of Biochemistry, University of Oxford, OX1 3QU, UK

[3] LICAMM, University of Leeds, LS2 9JT, UK

[4] Stem Cell Institute, University of Cambridge, CB2 1QR, UK

[5] LIMM, University of Leeds, LS9 7TF, UK

* Present address: Department of Genetics, Cambridge CB2 3EH, UK

** Present address: Wellcome Trust Centre for Human Genetics, Oxford, OX3 7BN, UK

Correspondence: dawn.coverley@york.ac.uk

Running Title: CIZ1 at the inactive X

Keywords: CIZ1; *Xist*; X-chromosome inactivation; nuclear matrix; lympho-proliferative disorder

Abstract

The nuclear matrix protein Cip1-interacting zinc finger protein 1 (CIZ1) promotes DNA replication in association with cyclins, and has been linked with adult and pediatric cancers. Here we show that CIZ1 is highly enriched on the inactive X chromosome (Xi) in mouse and human female cells, and is retained by interaction with the RNA-dependent nuclear matrix. CIZ1 is recruited to Xi in response to expression of Xist RNA during the earliest stages of X-inactivation in embryonic stem cells, and is dependent on the C-terminal nuclear matrix anchor domain of CIZ1 and the E-repeats of *Xist*. CIZ1 null mice, although viable, display fully penetrant female specific lymphoproliferative disorder. Interestingly, in MEF cells derived from CIZ1 null embryos Xist RNA localisation is disrupted, being highly dispersed through the nucleoplasm rather than focal. Focal localisation is reinstated following re-expression of CIZ1. Focal localisation of Xist RNA is also disrupted in activated B and T cells isolated from CIZ1 null animals, suggesting a possible explanation for female specific lymphoproliferative disorder. Together, these findings suggest that CIZ1 has an essential role in anchoring *Xist* to the nuclear matrix in specific somatic lineages.

Introduction

In mammals, dosage compensation for X-linked transcripts is achieved by the developmentally regulated inactivation of one of the two X chromosomes in female cells. X chromosome inactivation (XCI) is initiated by X-inactive specific transcript (*Xist*), a non-coding RNA approximately 17kb in length (Brockdorff et al. 1992; Brown et al. 1992; Lee et al. 1996; Penny et al. 1996). Xist RNA is expressed from the inactive X chromosome (Xi) elect and accumulates in cis to form a domain over the entire chromosome, serving as a trigger for a cascade of chromatin modifications that result in the progressive transition towards a stable, heritable, repressed state (reviewed in (Heard and Disteche 2006).

Analysis of *Xist* transgenes has revealed that *Xist*-mediated chromosome silencing and Xist RNA localisation are conferred by distinct elements (Wutz et al. 2002). Silencing activity maps in large part to the A-repeat, a short tandemly repeated region located at the 5' end of *Xist*. In contrast, localization maps to several redundantly acting elements, including the tandem repeat regions C, E and F (Wutz et al. 2002; Jeon and Lee 2011; Makhlouf et al. 2014; Yamada et al. 2015).

Xist spreading occurs through a sequence of events dictated by the architecture of the X chromosome. Xist RNA searches for binding sites in three dimensions, leading to modification of chromosome structure, before spreading to newly accessible locations (Engreitz et al. 2013; Simon et al. 2013). While the nature of Xist RNA binding sites is poorly defined, it is known that Xist RNA localizes to the perichromatin compartment that corresponds to the nuclear matrix (NM) (Clemson et al. 1996; Smeets et al. 2014). Accordingly, the NM proteins scaffold attachment factor A (SAF-A, hnRNPU) and

hnRNP UL1 are involved in anchoring Xist RNA within the Xi (Helbig and Fackelmayer 2003; Hasegawa et al. 2010; Sakaguchi et al. 2016). Additionally, nuclear matrix protein 1 (NMP1, YY1) (Guo et al. 1995) has been implicated in tethering Xist RNA to chromatin (Jeon and Lee 2011; Makhlouf et al. 2014). In naïve B and T cells Xist RNA is dispersed in the nucleoplasm, but is recruited to Xi upon lymphocyte activation in a process that involves YY1 and SAF-A (Wang et al. 2016).

Recent proteomic and genetic screens have identified several novel *Xist* interacting factors, some of which now have confirmed roles in *Xist*-mediated silencing (Chu et al. 2015; McHugh et al. 2015; Moindrot et al. 2015; Monfort et al. 2015). With the exception of SAF-A identified previously (Hasegawa et al. 2010), none of the factors investigated in detail were found to affect *Xist* localisation (Chu et al. 2015; McHugh et al. 2015).

Random XCI of the paternal or maternal chromosome occurs around embryonic day 5.5, and is propagated through subsequent cell divisions. This can be recapitulated in XX mouse embryonic stem cells (ESCs), allowing fine-tuned analysis of timing and the earliest events in the initiation process. Examples include deposition of histone 3 lysine 27 trimethylation (H3K27me3), and hypoacetylation of H4, which occur rapidly at the onset of Xist RNA expression, and DNA methylation of promoters of X-linked genes and association of the variant histone macroH2A, which occur at later stages of the XCI process (Pollex and Heard 2012). *Xist*-dependent silencing occurs within a developmental window of opportunity corresponding to early stages of differentiation in the XX ESC model (Wutz and Jaenisch 2000). Beyond this time XCI enters a maintenance phase in which *Xist* is largely dispensable (Brown and Willard 1994; Csankovszki et al. 1999) despite continued expression.

Here we define a novel *Xist* localisation factor, the NM protein Cip1-interacting zinc finger protein 1 (CIZ1). CIZ1 was previously characterised as a factor with roles in initiation of DNA replication (Coverley et al. 2005), interacting directly with CDK2, p21/CIP1 (Mitsui et al. 1999), and cyclins (Copeland et al. 2010), and supporting cyclin recruitment to the NM (Copeland et al. 2015). The NM-anchor domain in the C-terminal third of CIZ1 (Ainscough et al. 2007) mediates immobilization of CIZ1 and its interaction partners, but retains the ability to become incorporated into the NM in the absence of cyclin cargo. CIZ1 has also been linked with post-replicative functions in male germ cell differentiation (Greaves et al. 2012). *CIZ1* transcripts are alternatively spliced to yield at least 22 variants (Rahman et al. 2010), of which most are not characterised. Aberrant alternative splicing underlies its links with a range of pathologies, including pediatric tumours and common adult onset cancers of the breast (den Hollander et al. 2006) and lung (Higgins et al. 2012), as well as neurological abnormalities (Xiao et al. 2016). Here we describe *Xist*-dependent recruitment of CIZ1 to Xi, and a requirement for CIZ1 to maintain Xist RNA localisation at Xi in fibroblasts and splenocytes.

Results

CIZ1 accumulates at Xi in female cells

Immuno-localization of endogenous CIZ1, via epitopes in its N-terminal DNA replication domain (Coverley et al. 2005; Copeland et al. 2010) or C-terminal NM anchor domain (Ainscough et al. 2007) (Fig 1A), reveal one or two high-intensity domains within the

nucleus of female human or mouse cultured fibroblasts, plus smaller nucleus-wide foci in both male and female cells (Fig 1B, Fig S1A). In immortalized, or primary embryonic fibroblasts (PEFs) CIZ1 domains are discrete, while in cancer-derived cell lines they are more irregular (shown for MCF7 breast cancer cells in Fig S1A). We hypothesised that the high intensity domains present only in female cells correspond to Xi. Consistent with this, immuno-staining of H3K27me3, a marker for Xi, co-localises with CIZ1 in PEFs (Fig 1B), and a range of other female cell types (Fig S1A). CIZ1 did not co-localise with the active chromatin mark H3K4me3 or constitutive heterochromatin mark H3K9me3 (Fig S1B). Identification of the CIZ1 domains observed in female PEFs as the silenced X-chromosome was confirmed by immuno-FISH for CIZ1 and Xist RNA (Fig 1C), which revealed localisation within the same chromosome territory.

To determine at which stage of the XCI process CIZ1 is recruited we analysed CIZ1 localisation in PGK12.1 XX mESCs at time points following initiation of differentiation. CIZ1 localisation to Xi was observed from day 1 and persisted throughout the time course (Fig 1D, Fig S1C). This closely correlates with the dynamics of Xist RNA expression reported previously (Sheardown et al. 1997). As in PEFs, CIZ1 domains co-localised with H3K27me3 identifying their location as Xi. CIZ1 is lost from Xi in late metaphase in both ESCs (Fig 1E) and PEFs (Fig S1D), indicating a cycle of recruitment and loss that is similar to Xist RNA (Duthie et al. 1999). The smaller nucleus-wide foci remain qualitatively similar throughout ESC differentiation, but in late metaphase are excluded from chromosomes (Fig S1D and (Greaves et al. 2012).

Super-resolution three-dimensional structured illumination microscopy (SR 3D-SIM) of endogenous CIZ1 together with endogenous Xist RNA in diploid female somatic C127I

cells confirmed their adjacent localization, similar to that for SAF-A (Smeets et al. 2014),(Fig 2A, Fig S2B).

Nuclear Matrix association of CIZ1 at Xi

The NM is a biochemically defined fraction that resists extraction from the nucleus, and which is thought to anchor and spatially organise nuclear processes including DNA replication and repair, transcription and pre-mRNA splicing (Wilson and Coverley 2013). Serial extraction (Wilson et al. 2016) to reveal the fraction of CIZ1 that remains in cells after solubilisation with i) low-level detergent under physiological salt concentrations, ii) 0.5M salt, iii) nuclease (DNase or RNase) (Fig 2B), revealed distinct populations in female 3T3 cells (Fig 2C) and PEFs (Fig S2C). While the small nucleus-wide foci remained under all conditions (part of the core protein NM), the high-intensity domain at Xi was released by digestion with RNase, but not DNase. This resistance to high-salt and DNase defines CIZ1 at Xi as part of the NM, but release by RNase shows this to be the RNA fraction of the NM, and is consistent with its close association with Xist RNA.

When 3T3 cells were treated with the protein-protein cross-linker DTSP prior to extraction (Fig 2D), the CIZ1 domain at Xi was rendered resistant to digestion with RNase. This, suggests it to be in close proximity to proteins in the core NM, possibly the resistant fraction of CIZ1. Thus, two qualitatively different populations of NM-anchored CIZ1 are present in the nucleus, but most of the CIZ1 at Xi is anchored by association with RNA (Fig 2E).

Similar analysis of the NM proteins SAF-A and YY1 in 3T3 cells showed that they are not enriched at Xi, that a NM-associated population can be revealed by removal of chromatin, and that both proteins are completely extracted by digestion of RNA (Fig S3).

All three of these features are consistent with the published literature, but distinguish SAF-A and YY1 from CIZ1.

Recruitment to Xi requires CIZ1 C-terminal nuclear matrix anchor domain

To ask whether recruitment of CIZ1 to Xi is mediated by the sequences that support attachment to the NM (Ainscough et al. 2007), the C-terminal anchor domain (GFP-C275, which includes C2H2 type zinc fingers and matrin 3-type RNA-binding zinc finger domains), and the N-terminal DNA replication domain (GFP-N572, which includes CDK phosphorylation sites and cyclin binding motifs), were separately transiently transfected into 3T3 cells and the frequency of accumulation at the Xi territory scored after one cell cycle. N572 completely failed to accumulate at Xi, while C275 accumulated in large foci that colocalized with endogenous CIZ1 at Xi (Fig 3A). However compared to GFP-full length CIZ1 the frequency of C275 marked X-chromosomes was significantly reduced, despite presence in the nucleus. Thus, while sequences encoded in N572 are not sufficient to specify recruitment to Xi on their own, they do increase efficiency of targeting. When stably transfected into the P4D7F4 XY mESC line which carries an mCherry tagged inducible *Xist* transgene (Moindrot et al. 2015), live cell imaging revealed (in cells with sufficient expression of both markers) co-localisation between C275 and Xist RNA domains, whereas N572 showed no *Xist* co-localization (Fig 3B). Together, these findings support a key role for the C-terminus of CIZ1 in binding at Xi.

Recruitment of CIZ1 by *Xist* requires the *Xist* E-repeat region

In undifferentiated male MG-3E (XY) ESCs carrying an inducible *Xist* transgene CIZ1 is recruited to the *Xist* domain and shows a similar adjacent localization to *Xist* as in female ESCs (Fig S4A). To define elements in Xist RNA required for CIZ1 recruitment

we analysed a series of inducible transgenic *Xist* deletion constructs in XY ESCs (Fig 3C and Fig S5), and a deletion of *Xist* exon IV from the endogenous *Xist* locus in female MEFs (Fig S4B) (Caparros et al. 2002). The deletions encompassed key elements, including six short tandem repeat regions (A-F) (Brockdorff et al. 1992; Brown et al. 1992; Nesterova et al. 2001), which are conserved and in some cases have been shown to be functionally important. CIZ1 recruitment was found to be independent of the A-repeat region, which is required for *Xist*-mediated silencing (Wutz et al. 2002), and the XN region (repeats B and F), which is involved in recruitment of PRC2 to Xi (da Rocha et al. 2014) (Fig 3C). However a truncated Xist construct, which corresponds to the first 3 kb of *Xist* does not recruit CIZ1, implicating regions further 3'. Accordingly, deletion of the E repeats, encompassing a 1.5 kb span of *Xist* exon 7, entirely abolished CIZ1 recruitment by Xist RNA (Fig 3D). Deletion of other 3' regions, the D repeats or the highly conserved *Xist* exon 4 had no effect (Fig 3C, D). These findings demonstrate a requirement for *Xist* E-repeats for recruitment of CIZ1, and together raise the possibility that the C-terminus of CIZ1 might functionally interact with Xist RNA via the E-repeat region.

Functional analysis of CIZ1 in X chromosome inactivation

Loss of function mutations affecting factors critical for XCI, including Xist RNA, result in female specific lethality, usually during early- or mid-stages of embryogenesis. To determine if this is the case for CIZ1, targeted C57BL/6 ES cells generated using a gene trap strategy were used to produce heterozygous knockout mice (Fig S6A, B). Viable CIZ1-/- male and female F1 progeny were born at the expected ratio (Table S1), showed no difference in growth rate and had no overt developmental defects. Loss of CIZ1

transcript was confirmed in embryos (E12), and fibroblasts from three-week post-natal tail tip dermal tissue (TTFs) (Fig S6C). Loss of protein expression was confirmed in TTFs and lymphocytes (Fig S6D, E) and in differentiating male germ cells, which normally express high levels of CIZ1 (Greaves et al. 2012) (Fig S6F). Thus, the gene trap insertion abrogates expression from the CIZ1 locus in vivo and in vitro, demonstrating that CIZ1 is not essential for embryogenesis, early post-natal development, or cell viability ex vivo.

The absence of an embryonic phenotype suggests that CIZ1 is not required for the establishment of a transcriptionally quiescent, inactivated X chromosome, despite recruitment during *Xist*-dependent initiation of X-inactivation (Fig 1D). Consistent with this the transcriptome of CIZ1 null-derived female PEFs did not reveal widespread reactivation of the Xi compared to WT controls (data set S1, Fig 4A). As expected the *Ciz1* gene was silenced in null cells (p=5.00E-05; q=0.005, data set S2), but comparison of all transcripts that map to the X-chromosome of the Mus_musculus C57BL/6 primary assembly GRCm38 (downloaded from Ensembl.org on 4/05/2016) showed that most were not significantly altered, and revealed little change in genes associated with the XIC (Fig 4B). Lack of widespread reactivation is in line with similar analyses, and the understanding that loss of Xist RNA or other factors does not significantly compromise maintenance of XCI (Csankovszki et al. 1999).

However deregulation at the single gene level was significant ($P<0.05$) for 62 X-linked transcription units dispersed across the X. This is 3.6% of those that are expressed in PEFs and includes a similar number of up and down-regulated genes, and six where $q< 0.05$; *Agtr2*, *Fhl1*, *Tmem164*, *Gpm6b*, XLOC3750 and XLOC830 (data set S2). Induction

of full-length GFP-CIZ1 transgene in PEFs derived from CIZ1 null line E13.17 harbouring an inducible CIZ1 transgene and doxycycline regulatable transactivator (see supplemental materials and methods), re-balanced expression of all six genes, modulating four of them back to WT levels (Fig 4C). Thus, expression of full-length CIZ1 compensates for genetic ablation, and presumptive loss of the full repertoire of *Ciz1* variant transcripts in the regulation of these genes.

Lympho-proliferative disorder in adult female mice

Although we observed no overt defects in embryogenesis or early post-natal development (Fig 5), progressive infirmity was observed in female CIZ1 null mice from 9 months onwards. Eight females and an equivalent number of males were therefore evaluated for abnormalities between 9 and 19 months. This revealed lympho-proliferative disorder in all 8 females and in none of the males. Detailed histological assessment was undertaken for 6 of the females, and compared to 6 WT females. Summary assessment of abnormalities in spleen, liver, lung and lymph node for individual CIZ1 null and WT females is given in Table S2, and pathology notes describing histological assessments are in Tables S3 and S4. Notably, primary and secondary lymphoid tissues (spleen, lymph node, lung, and liver) were enlarged in all *Ciz1*-/- adult females (Fig 5C). Secondary lymphoid tissues are sites where B and T lymphocytes are directed in search of antigen, leading to regulated turnover or amplification of subsets of cells within germinal centres. This process is deregulated most notably in the spleen (Fig 5C, D), which displayed a 5-fold enlargement in *Ciz1*-/- (181-3679mg) compared to *Ciz1*+/+ (88-167mg) mice. Histologically, lymph node and spleen architecture were abnormal, with effacement of normal follicles, and significant

infiltration of abnormal B (CD20 +ve) and reactive T (CD3 +ve) lymphocytes in all affected tissues (Fig 5D, E). At the cellular level the disorder resembled non-Hodgkin follicular type lymphoma, with three showing evidence of high-grade transformation consistent with diffuse large B cell lymphoma (Ward 2006). These data point to compromised X chromosome inactivation in lymphoid lineages, and suggest that CIZ1 normally protects against tumor formation.

CIZ1 is required for Xist RNA localisation in fibroblasts and splenocytes

While the viability of CIZ1 null embryos suggests that CIZ1 is not critical for the establishment of XCI, female-specific lymphoid hyper-proliferation nevertheless implies an important lineage restricted function. To further investigate this we performed RNA FISH to analyse *Xist* domains in PEFs and splenocytes derived from CIZ1 null mice. In independently derived CIZ1 null fibroblast cell lines, we observed a strikingly dispersed *Xist* signal that occupies 40% of the nuclear area compared to less than 5% in WT cells, and also loss of H3K27me3 (Fig.6A). Dispersal cannot be attributed to increased *Xist* levels as none of the three CIZ1 null PEFs showed any change in *Xist* transcript (data set S1). X-chromosome paints showed no significant difference between WT and CIZ1 null PEFs (Fig 6B), suggesting that there is a deficit in Xist RNA localisation rather than Xi organisation.

Further substantiating the conclusion that CIZ1 plays a role in Xist RNA localisation, induction of full-length GFP-CIZ1 transgene (Fig 6C, D, E) fully reinstated localisation of Xist RNA over Xi domains (Fig 6F, G). Prior to induction of CIZ1, *Xist* was dispersed in over 80% of CIZ1 null E13.17 PEFs, but became re-localized to discrete domains that overlap with GFP-CIZ1 domains within 20 hours (Fig 6H). Together these observations

demonstrate that CIZ1 plays a key role in Xist RNA localisation in primary embryonic fibroblasts.

In light of the female specific lymphoproliferative disorder observed in CIZ1 null animals, we went on to investigate the role of CIZ1 in X inactivation in haematopoetic lineages. We evaluated the impact of CIZ1 deletion in splenocytes from six-week old females, after stimulation of mixed populations of naïve B/T cells with either the B-cell activator lipopolysaccharides (LPS) or T-cell activator αCD3 antibody (αCD3). Consistent with a previous report (Wang et al. 2016) activation of both cell types from WT mice induced dramatic focal localisation of *Xist* to Xi within 24 hours, and this was mirrored by accumulation of CIZ1 (Fig 7). However, activated B and T lymphocytes from CIZ1 null mice failed to show appropriate Xist RNA localisation (Fig 7B). This finding identifies a transition point in the affected lineages that is compromised in CIZ1 null animals. To ask whether aberrant *Xist* localisation leads to relaxed control over X-linked genes we compared the transcriptome of WT spleen (containing mostly naïve cells), and CIZ1 null spleen (containing hyperproliferative cell populations likely expanded from rare activated precursors) from adult mice. Overall, from the 2209 X-linked genes that returned test data (Fig S7A, data set S2), 16.4% were up-regulated and 8.7% down regulated by greater than 2 fold (Fig S7B). As expected, whole genome gene set enrichment analysis returned highly significant overlap with immunological processes and cell division gene ontology terms (Fig S7C, data set S3). Comparison of the X-linked genes to the gene list reported to be upregulated in blood cells of *Xist* mutant mice (Yildirim et al. 2013) showed that many of the same genes are affected (Fig S7D, data set S4), however a similar proportion of genes were affected genome-wide (Fig S7B). Together the data

demonstrate that CIZ1 plays a key role in stabilising *Xist* association with Xi in lymphoid lineages, but that its effects are not limited to the X chromosome.

Discussion

Here we demonstrate that the NM protein CIZ1 is strongly enriched over the inactive X chromosome territory. Although CIZ1 was not previously linked to XCI, one of four recent screens identified CIZ1 amongst 81 candidate *Xist* interactors (Chu et al. 2015). Based on our findings, a relationship between CIZ1 and *Xist* is clear, though whether localisation of CIZ1 to Xi domains is attributable to a direct interaction with Xist RNA, or to an interaction with other *Xist* or Xi-bound factors remains to be seen. Several observations support a functional interaction. First, loss of CIZ1 results in dispersal of *Xist* in somatic cells. Second CIZ1 enrichment occurs rapidly at the onset of Xist RNA expression, and is present in all observed cases where Xist RNA domains are observed. Third, SR 3D-SIM analyses demonstrates that CIZ1 and Xist RNA lie in very close proximity, and that CIZ1 is localised to the RNA-dependent NM compartment at Xi. Finally, the C-terminus of CIZ1, which anchors it at Xi, encompasses known RNA binding domains, notably the Matrin3 type Zn finger, suggesting a possible direct interaction. Interestingly, Matrin3 has also been identified as a candidate *Xist* interactor (Chu et al. 2015; Moindrot et al. 2015). Further studies are nevertheless required to determine if there is a direct interaction between CIZ1 and Xist RNA, specifically the E-repeat region, and we cannot at this stage rule out that CIZ1 recognises another *Xist*-interacting protein, for example PTBP, recently shown to bind the E-repeat region (Chen et al. 2016).

Several studies have pointed to a role for the NM in anchoring Xist RNA within the Xi territory, and a number of other proteins that interact with the NM, or with DNA sequences that interact with the NM (S/MARs), have been implicated in XCI including SAF-A, YY1 and SATB1. SAF-A and CIZ1 are similar in that their ability to support *Xist*-mediated gene silencing, and recruitment of *Xist* to Xi respectively, is dependent on *Xist* E repeats (Hasegawa et al. 2010), possibly identifying a common mechanism. Moreover, deletion of the E-repeats was recently shown to result in dispersed localisation of Xist RNA (Yamada et al. 2015). These findings were attributed to SAF-A, however our results suggest that loss of interaction with CIZ1 might contribute to the observed phenotype. Notably, sensitivity of both SAF-A and YY1 to digestion of the RNA component of the NM distinguish them from CIZ1, which is part of the core protein matrix throughout the nucleus, suggesting important differences in their roles.

Scaffolding the structural reorganization of the Xi during XCI, or maintenance of compacted structure, are possible functions for the NM to which CIZ1 might contribute. Another possibility, suggested by the function of CIZ1 in DNA replication, is regulatable recruitment of factors into or away from the Xi territory. During late G1 phase CIZ1 supports recruitment of cyclin A to the NM. Cyclin docking on CIZ1, but not CIZ1 recruitment to the NM, is switched off at S phase (Copeland et al. 2015). Thus, in the context of DNA replication CIZ1 appears to be a cargo carrier or mediator that is sensitive to cell cycle stage, raising the possibility of a relationship with cell cycle regulators implicated in *Xist* retention (Hall et al. 2009).

Although our observations in PEFs and lymphocytes implicate CIZ1 in anchoring *Xist* to the NM, the fact that CIZ1 null females are viable implies that the same relationship

might not apply during early embryogenesis. Based on this, we hypothesise that CIZ1 functions redundantly with other anchoring factors, for example SAF-A, and that these are sufficient during embryogenesis but insufficient in PEFs or lymphocytes. A recent report suggested that SAF-A is not essential for *Xist* localisation in all lineages, and that other factors may compensate for its loss (Kolpa et al. 2016). However, this contrasts with genetic depletion of SAF-A in MEFs, which showed a requirement for SAF-A (Sakaguchi et al. 2016). Thus, the relationship between CIZ1 and SAF-A is not known and there may be more factors capable of anchoring *Xist* at Xi.

Here we show that recruitment of *Xist* upon stimulation of lymphoid lineages (Wang et al. 2016) is dependent on CIZ1, describing a role for CIZ1 in a lineage-restricted transition that occurs throughout the lifetime of the mouse. An *Xist*-dependent silencing pathway was previously reported to be transiently activated during haematopoetic differentiation (Savarese et al. 2006), with pre-B and pre-T cells the most dependent. This aligns closely with our observation of B and T cell hyperplasia in CIZ1 null mice, and is consistent with independent analysis that described susceptibility to oncogene-induced transformation leading to leukemias in the absence of CIZ1, though no sex bias was reported in this study (Nishibe et al. 2013).

We observed widespread deregulation of gene expression in the absence of CIZ1 in affected lineages, though this was not specific to the X-chromosome. However, we cannot rule out that low level reactivation of multiple X-linked genes together, considered collectively, confers the female specific lymphoproliferation phenotype. Thus it remains an open question whether the disorder observed in CIZ1 null mice is a consequence of compromised X chromosome inactivation. Proliferative disorders of the

haematopoetic system have been associated with deletion or suppression of factors linked with XCI (Leong et al. 2013) (Yildirim et al. 2013), and abnormalities of XCI are frequently reported in cancers including duplication of the active X (Xa) in breast and ovarian cancers and leukemias (Spatz et al. 2004; Lee and Bartolomei 2013). However, X chromosomes carry proportionally more immune-related genes than the rest of the genome (Bianchi et al. 2012), which means that a more general failure of control of gene expression might manifest preferentially in females. Transcriptome analysis in PEFs identified candidate X-linked drivers of haematopoetic malignancies; *Gpm6b* overexpression is linked with B-cell lymphoma (Charfi et al. 2014), and *Figf*, (VEGF-D) is implicated in the metastatic spread of tumours via lymph nodes (Pazgal et al. 2007) (Bardelli et al. 2007). However, we interpret this with caution because changes elsewhere in the genome, initiated directly or indirectly as a consequence of loss of CIZ1, are also likely to play a role.

In conclusion we have defined a novel component of the X inactivation pathway, the NM protein CIZ1. Our results indicate that CIZ1 functionally interacts with Xist RNA via the E-repeat region, and moreover that CIZ1 facilitates in cis-localisation of Xist RNA, functioning as an anchor to the NM in somatic cell lineages.

Materials and Methods

Further details are available in Supplemental Materials and Methods.

Animals and genotyping All animal work was carried out under UK Home Office licence. CIZ1 null mice were generated from C57BL/6 ES clone IST13830B6 (TIGM)

harboring a neomycin resistance gene trap inserted downstream of exon 1. Absence of *Ciz1*/CIZ1 in homozygous progeny was confirmed by qPCR, immunofluorescence and immunoblot with CIZ1 N-term antibody. Inducible *GFPCiz1*-Tg mice, generated by pronuclear injection of a GFP full-length *Ciz1* construct into CBA/C57BL6 fertilized eggs, were crossed with ROSA26-rtTA mice (Jackson labs). All primers used for characterisation of *Ciz1* targeting and for detection of transactivator and responder transgenes, and sex, are in Supplemental Materials and Methods.

Cell Lines All stable cell lines were grown following standard procedures. Mouse Primary Embryonic Fibroblasts (PEFs) were derived from individual embryos at day 13-14 of gestation. Primary Tail Tip Fibroblasts (TTFs) were generated from individual 3-week old mice. Genotype and sex were confirmed after explant culture, using primers given in Supplemental Materials and Methods. For inducible cells harbouring ROSA26-rtTA and *GFPCiz1*-Tg transgenes addition of doxycycline to media (5 μg/ml) was used to induce detectable GFP-CIZ1 within 6 hours. ES cells were grown on feeders with addition of LIF. Where applicable *Xist* expression was induced with doxycycline at 1.5μg/ml. Male XY P4D7 ES cells, derived from the cross between C57BL/6JJcl and 129+*Ter*/SvJcl, and containing an rtTA cassette in the ROSA26 locus (Mondroit et al., 2015), were used to generate stable autosomal integrants of *Xist* inducible deletion variants.

Splenocyte isolation and activation Spleens isolated from 6-week old WT and *Ciz1* null females were pressed through 70 um nylon filters to dissociate naïve B and T lymphocytes into media (RPMI 1640 (Invitrogen) supplemented with 10% foetal calf serum, 100u/ml Penicillin, 10 μg/ml Streptomycin and 2 mM L-glutamine).

The cells were pelleted at 450g for 5 mins, then resuspended in red blood cell lysis solution (Sigma) for 3 min before pelleting and resuspending in 2 ml media. The cell suspensions were counted with trypan blue to determine viability, and adjusted to 10 x 10^6 cells/ml. 100 ul (1 x 10^6 cells) was transferred into individual wells of a 96 well plate and supplemented with 100 ul of (i) media for unactivated control, (ii) 1 ug/ml Lipopolysaccharides (LPS - Sigma) for B-cell activation, or (iii) 1 ug/ml αCD3 (BioLegend) for T-cell activation. After 24-48 hours the cells were processed for RNA-FISH, immunofluorescence and protein isolation.

Whole genome RNA sequencing and Bioinformatics. In brief, cell lines (detailed in Supplemental Materials and Methods) were grown to 80% density before RNA extraction and DNaseI treatment. Libraries, optimised for 250-400 bp inserts, were prepared using NEBNext® Ultra™ (Illumina®), enriched for mRNA using NEBNext Poly(A) mRNA Magnetic Isolation Module, and sequenced to generate ~5x10^7 reads per sample. STAR software was used to align reads to the C57BL/6 X-chromosome. Transcriptome assembly and expression quantification were performed using Cufflinks and Cuffdiff. Of 85 differentially expressed X-linked transcription units ($p<0.05$) 23 were excluded due to differential expression between biological replicates. Heat maps and gene enrichment analysis were carried out as described in Supplemental Materials and Methods.

Histology Following dissection tissues were transferred immediately into histological grade formalin and processed after 24-48 hrs. Immunostaining for CD antigens was performed using Rabbit anti-CD3 for T cells (Abcam ab16669) at 1:200 and Goat anti-CD20 for B cells (Santa Cruz sc7735) at 1:500.

ES cell differentiation Female PGK12.1 ES cells were grown in ES media with LIF on gelatin without feeders. To induce differentiation $1x10^6$ cells were plated onto non-gelatinised dishes without LIF. On day 3 differentiating colonies were replated onto bacterial dishes to stimulate embryoid body (EB) formation. On day 7 EBs were transferred to non-gelatinised dishes to reattach. Fibroblast outgrowths were passaged as required.

Nuclear Matrix extraction Cells were serially extracted with (i) detergent, to reveal soluble factors, (ii) salt, to reveal loosely bound chromatin associated factors, (iii) DNaseI, to reveal tightly attached chromatin associated factors, and (iv) RNase, to reveal RNA associated factors, as described (Wilson et al. 2016), with improvements detailed and in Supplemental Materials and Methods. Coverslips were then fixed and processed for immunofluorescence.

Immunofluorescence Cells were washed in PBS and either (i) fixed in 4% PFA to reveal total protein, or (ii) treated with detergent prior to fixing to reveal chromatin and NM associated factors, prior to incubation with primary antibody for 2hrs then secondary antibody for 1hr. For ES cell differentiation course PGK12.1 cells were fixed in 2% formaldehyde for 15 min prior to permeabilisation. Antibodies used were α-H3K27me3 mAb (Abcam ab6002, Active Motif ab61017), α-CIZ1 N-Term (1794), α-CIZ1 C-term (Novus NB100-74624), SAFA - Abcam anti HNRNP-U (ab10297), anti-YY1 (SC7341). Coverslips were co-stained with limiting concentrations of Hoechst 33258 10ng/ml (Sigma), for quantitative detection of chromatin.

RNA-FISH: Female cultured cells were processed for detection of *Xist* transcript (red) by RNA-FISH, followed by immuno-FISH for CIZ1 (green) using N-term antibody 1794. An

11 kb Spe1-Sal1 mouse *Xist* fragment was fluorescently tagged with Cy3-dUTP (GE Healthcare) using BioPrime labelling kit (Invitrogen). Samples were incubated with probe overnight at 37C. For subsequent detection of CIZ1, antibody 1794 was applied for 1 hour, followed by secondary anti-rabbit FITC (Sigma) for 1 hour. Cells were imaged and processed using Adobe Photoshop CS4 to enhance signal definition. Prior RNA-FISH processing resulted in reduced CIZ1 signal intensity throughout the nucleus. For SR-3DSIM *Xist* cDNA was labelled with green-dUTP by nick translation (Abbott Molecular). Following fixation and permeabilisation cells were incubated with primary antibody for 1 hour, then with Alexa Fluor goat anti-rabbit 594 for 30min, then washed and post-fixed before detection of *Xist* overnight. After extensive washing the cells were incubated with 2µg / ml DAPI and mounted with Vectorshield.

Chromosome paints FITC conjugated X chromosome paint (AMP 0XG) was used as instructed (Cytocell Ltd Cambridge). Labelled cells were mounted in vectorshield with DAPI and imaged.

Microscopy Images were collected using a Zeiss Axiovert 200M, Axiocam and Openlab image acquisition software, and quantified using ImageJ (NIH) using raw images acquired under identical conditions. Images for publication were enhanced using Adobe Photoshop or Affinity Photo 1.4 by applying identical manipulation to test and control samples so that image intensities reflect actual relationships. Live images were collected on PE Ultraview spinning disk confocal microscope. Super-resolution 3D-SIM was performed on a DeltaVision OMX V3 Blaze system (GE Healthcare) equipped with a 60x/1.42 NA PlanApo oil immersion objective (Olympus), sCMOS cameras (PCO),

and 405, 488 and 593nm lasers. 3D-SIM image stacks were acquired as described in supplementary Information.

Acknowledgements Work was supported by Radhika Sreedhar Scholarship to RR-F, University of York priming funds, BBSRC PhD training scholarships to ES and RW, Genetics Society training funds to RR, Wellcome Trust grants to NB (081385,091911) and the Micron advance imaging initiative (Wellcome Trust 103768). X-chromosome paints were a kind gift from Cytocell. We are grateful to James Hewitson, Dimitris Lagos, Mike Shires and Matthew Wiseman for advice or assistance, and to Sally James, Richard Randle-Boggis, Katherine Newling and Peter Ashton of York Technology Facility Genomics laboratory.

References

Agrelo R, Souabni A, Novatchkova M, Haslinger C, Leeb M, Komnenovic V, Kishimoto H, Gresh L, Kohwi-Shigematsu T, Kenner L et al. 2009. SATB1 defines the developmental context for gene silencing by Xist in lymphoma and embryonic cells. *Dev Cell* **16**: 507-516.

Ainscough JF, Rahman FA, Sercombe H, Sedo A, Gerlach B, Coverley D. 2007. C-terminal domains deliver the DNA replication factor Ciz1 to the nuclear matrix. *Journal of Cell Science* **120**: 115-124.

Bardelli M, Leucci E, Schurfeld K, Bellan C, Passiatore G, Rocchigiani M, Bartolommei S, Orlandini M, Zagursky J, Lazzi S et al. 2007. VEGF-D is expressed in activated lymphoid cells and in tumors of hematopoietic and lymphoid tissues. *Leuk Lymphoma* **48**: 2014-2021.

Bianchi I, Lleo A, Gershwin ME, Invernizzi P. 2012. The X chromosome and immune associated genes. *Journal of autoimmunity* **38**: J187-192.

Brockdorff N, Ashworth A, Kay GF, McCabe VM, Norris DP, Cooper PJ, Swift S, Rastan S. 1992. The product of the mouse Xist gene is a 15 kb inactive X-specific transcript containing no conserved ORF and located in the nucleus. *Cell* **71**: 515-526.

Brown CJ, Hendrich BD, Rupert JL, Lafreniere RG, Xing Y, Lawrence J, Willard HF. 1992. The human XIST gene: analysis of a 17 kb inactive X-specific RNA that contains conserved repeats and is highly localized within the nucleus. *Cell* **71**: 527-542.

Brown CJ, Willard HF. 1994. The human X-inactivation centre is not required for maintenance of X-chromosome inactivation. *Nature* **368**: 154-156.

Caparros ML, Alexiou M, Webster Z, Brockdorff N. 2002. Functional analysis of the highly conserved exon IV of XIST RNA. *Cytogenet Genome Res* **99**: 99-105.

Charfi C, Edouard E, Rassart E. 2014. Identification of GPM6A and GPM6B as potential new human lymphoid leukemia-associated oncogenes. *Cell Oncol (Dordr)* **37**: 179-191.

Chen CK, Blanco M, Jackson C, Aznauryan E, Ollikainen N, Surka C, Chow A, Cerase A, McDonel P, Guttman M. 2016. Xist recruits the X chromosome to the nuclear lamina to enable chromosome-wide silencing. *Science*.

Chu C, Zhang QC, da Rocha ST, Flynn RA, Bharadwaj M, Calabrese JM, Magnuson T, Heard E, Chang HY. 2015. Systematic discovery of Xist RNA binding proteins. *Cell* **161**: 404-416.

Clemson CM, McNeil JA, Willard HF, Lawrence JB. 1996. XIST RNA paints the inactive X chromosome at interphase: evidence for a novel RNA involved in nuclear/chromosome structure. *The Journal of cell biology* **132**: 259-275.

Copeland NA, Sercombe HE, Ainscough JF, Coverley D. 2010. Ciz1 cooperates with cyclin-A-CDK2 to activate mammalian DNA replication in vitro. *Journal of Cell Science* **123**: 1108-1115.

Copeland NA, Sercombe HE, Wilson RH, Coverley D. 2015. Cyclin-A-CDK2-mediated phosphorylation of CIZ1 blocks replisome formation and initiation of mammalian DNA replication. *J Cell Sci* **128**: 1518-1527.

Coverley D, Marr J, Ainscough J. 2005. Ciz1 promotes mammalian DNA replication. *Journal of Cell Science* **118**: 101-112.

Csankovszki G, Panning B, Bates B, Pehrson JR, Jaenisch R. 1999. Conditional deletion of Xist disrupts histone macroH2A localization but not maintenance of X inactivation. *Nat Genet* **22**: 323-324.

da Rocha ST, Boeva V, Escamilla-Del-Arenal M, Ancelin K, Granier C, Matias NR, Sanulli S, Chow J, Schulz E, Picard C et al. 2014. Jarid2 Is Implicated in the Initial Xist-Induced Targeting of PRC2 to the Inactive X Chromosome. *Mol Cell* **53**: 301-316.

den Hollander P, Rayala SK, Coverley D, Kumar R. 2006. Ciz1, a novel DNA-binding coactivator of the estrogen receptor α, confers hypersensitivity to estrogen action. *Cancer Research* **66**: 11021-11030.

Duthie SM, Nesterova TB, Formstone EJ, Keohane AM, Turner BM, Zakian SM, Brockdorff N. 1999. Xist RNA exhibits a banded localization on the inactive X chromosome and is excluded from autosomal material in cis. *Hum Mol Genet* **8**: 195-204.

Engreitz JM, Pandya-Jones A, McDonel P, Shishkin A, Sirokman K, Surka C, Kadri S, Xing J, Goren A, Lander ES et al. 2013. The Xist lncRNA exploits three-dimensional genome architecture to spread across the X chromosome. *Science* **341**: 1237973.

Greaves EA, Copeland NA, Coverley D, Ainscough JF. 2012. Cancer-associated variant expression and interaction of CIZ1 with cyclin A1 in differentiating male germ cells. *J Cell Sci* **125**: 2466-2477.

Guo B, Odgren PR, van Wijnen AJ, Last TJ, Nickerson J, Penman S, Lian JB, Stein JL, Stein GS. 1995. The nuclear matrix protein NMP-1 is the transcription factor YY1. *Proceedings of the National Academy of Sciences of the United States of America* **92**: 10526-10530.

Hall LL, Byron M, Pageau G, Lawrence JB. 2009. AURKB-mediated effects on chromatin regulate binding versus release of XIST RNA to the inactive chromosome. *The Journal of cell biology* **186**: 491-507.

Hasegawa Y, Brockdorff N, Kawano S, Tsutui K, Tsutui K, Nakagawa S. 2010. The matrix protein hnRNP U is required for chromosomal localization of Xist RNA. *Dev Cell* **19**: 469-476.

Heard E, Disteche CM. 2006. Dosage compensation in mammals: fine-tuning the expression of the X chromosome. *Genes Dev* **20**: 1848-1867.

Helbig R, Fackelmayer FO. 2003. Scaffold attachment factor A (SAF-A) is concentrated in inactive X chromosome territories through its RGG domain. *Chromosoma* **112**: 173-182.

Higgins G, Roper KM, Watson IJ, Blackhall FH, Rom WN, Pass HI, Ainscough JF, Coverley D. 2012. Variant Ciz1 is a circulating biomarker for early-stage lung cancer. *Proceedings of the National Academy of Sciences of the United States of America* **109**: E3128-3135.

Jeon Y, Lee JT. 2011. YY1 tethers Xist RNA to the inactive X nucleation center. *Cell* **146**: 119-133.

Kolpa HJ, Fackelmayer FO, Lawrence JB. 2016. SAF-A Requirement in Anchoring XIST RNA to Chromatin Varies in Transformed and Primary Cells. *Dev Cell* **39**: 9-10.

Lee JT, Bartolomei MS. 2013. X-inactivation, imprinting, and long noncoding RNAs in health and disease. *Cell* **152**: 1308-1323.

Lee JT, Strauss WM, Dausman JA, Jaenisch R. 1996. A 450 kb transgene displays properties of the mammalian X-inactivation center. *Cell* **86**: 83-94.

Leong HS, Chen K, Hu Y, Lee S, Corbin J, Pakusch M, Murphy JM, Majewski IJ, Smyth GK, Alexander WS et al. 2013. Epigenetic regulator Smchd1 functions as a tumor suppressor. *Cancer Res* **73**: 1591-1599.

Makhlouf M, Ouimette JF, Oldfield A, Navarro P, Neuillet D, Rougeulle C. 2014. A prominent and conserved role for YY1 in Xist transcriptional activation. *Nat Commun* **5**: 4878.

McHugh CA, Chen CK, Chow A, Surka CF, Tran C, McDonel P, Pandya-Jones A, Blanco M, Burghard C, Moradian A et al. 2015. The Xist lncRNA interacts directly with SHARP to silence transcription through HDAC3. *Nature* **521**: 232-236.

Mitsui K, Matsumoto A, Ohtsuka S, Ohtsubo M, Yoshimura A. 1999. Cloning and characterization of a novel p21(Cip1/Waf1)-interacting zinc finger protein, ciz1. *Biochem Biophys Res Commun* **264**: 457-464.

Moindrot B, Cerase A, Coker H, Masui O, Grijzenhout A, Pintacuda G, Schermelleh L, Nesterova TB, Brockdorff N. 2015. A Pooled shRNA Screen Identifies Rbm15, Spen, and Wtap as Factors Required for Xist RNA-Mediated Silencing. *Cell Rep* **12**: 562-572.

Monfort A, Di Minin G, Postlmayr A, Freimann R, Arieti F, Thore S, Wutz A. 2015. Identification of Spen as a Crucial Factor for Xist Function through Forward Genetic Screening in Haploid Embryonic Stem Cells. *Cell Rep* **12**: 554-561.

Nesterova TB, Slobodyanyuk SY, Elisaphenko EA, Shevchenko AI, Johnston C, Pavlova ME, Rogozin IB, Kolesnikov NN, Brockdorff N, Zakian SM. 2001. Characterization of the genomic Xist locus in rodents reveals conservation of overall gene structure and tandem repeats but rapid evolution of unique sequence. *Genome Res* **11**: 833-849.

Nishibe R, Watanabe W, Ueda T, Yamasaki N, Koller R, Wolff L, Honda Z, Ohtsubo M, Honda H. 2013. CIZ1, a p21Cip1/Waf1-interacting protein, functions as a tumor suppressor in vivo. *FEBS Lett* **587**: 1529-1535.

Pazgal I, Boycov O, Shpilberg O, Okon E, Bairey O. 2007. Expression of VEGF-C, VEGF-D and their receptor VEGFR-3 in diffuse large B-cell lymphomas. *Leuk Lymphoma* **48**: 2213-2220.

Penny GD, Kay GF, Sheardown SA, Rastan S, Brockdorff N. 1996. Requirement for Xist in X chromosome inactivation. *Nature* **379**: 131-137.

Pollex T, Heard E. 2012. Recent advances in X-chromosome inactivation research. *Curr Opin Cell Biol* **24**: 825-832.

Rahman FA, Aziz N, Coverley D. 2010. Differential detection of alternatively spliced variants of Ciz1 in normal and cancer cells using a custom exon-junction microarray. *BMC Cancer* **10**: 482.

Sakaguchi T, Hasegawa Y, Brockdorff N, Tsutsui K, Tsutsui KM, Sado T, Nakagawa S. 2016. Control of Chromosomal Localization of Xist by hnRNP U Family Molecules. *Dev Cell* **39**: 11-12.

Savarese F, Flahndorfer K, Jaenisch R, Busslinger M, Wutz A. 2006. Hematopoietic precursor cells transiently reestablish permissiveness for X inactivation. *Molecular and cellular biology* **26**: 7167-7177.

Sheardown SA, Duthie SM, Johnston CM, Newall AE, Formstone EJ, Arkell RM, Nesterova TB, Alghisi GC, Rastan S, Brockdorff N. 1997. Stabilization of Xist RNA mediates initiation of X chromosome inactivation. *Cell* **91**: 99-107.

Simon MD, Pinter SF, Fang R, Sarma K, Rutenberg-Schoenberg M, Bowman SK, Kesner BA, Maier VK, Kingston RE, Lee JT. 2013. High-resolution Xist binding maps reveal two-step spreading during X-chromosome inactivation. *Nature* **504**: 465-469.

Smeets D, Markaki Y, Schmid VJ, Kraus F, Tattermusch A, Cerase A, Sterr M, Fiedler S, Demmerle J, Popken J et al. 2014. Three-dimensional super-resolution microscopy of the

inactive X chromosome territory reveals a collapse of its active nuclear compartment harboring distinct Xist RNA foci. *Epigenetics & chromatin* **7**: 8.

Spatz A, Borg C, Feunteun J. 2004. X-chromosome genetics and human cancer. *Nat Rev Cancer* **4**: 617-629.

Wang J, Syrett CM, Kramer MC, Basu A, Atchison ML, Anguera MC. 2016. Unusual maintenance of X chromosome inactivation predisposes female lymphocytes for increased expression from the inactive X. *Proceedings of the National Academy of Sciences of the United States of America* **113**: E2029-2038.

Ward JM. 2006. Lymphomas and leukemias in mice. *Exp Toxicol Pathol* **57**: 377-381.

Wilson RH, Coverley D. 2013. Relationship between DNA replication and the nuclear matrix. *Genes to Cells* **18**: 17-31.

Wilson RH, Hesketh EL, Coverley D. 2016. Preparation of the Nuclear Matrix for Parallel Microscopy and Biochemical Analyses. *Cold Spring Harb Protoc* **2016**: pdb prot083758.

Wutz A, Jaenisch R. 2000. A shift from reversible to irreversible X inactivation is triggered during ES cell differentiation. *Mol Cell* **5**: 695-705.

Wutz A, Rasmussen TP, Jaenisch R. 2002. Chromosomal silencing and localization are mediated by different domains of Xist RNA. *Nat Genet* **30**: 167-174.

Xiao J, Vemula SR, Xue Y, Khan MM, Kuruvilla KP, Marquez-Lona EM, Cobb MR, LeDoux MS. 2016. Motor phenotypes and molecular networks associated with germline deficiency of Ciz1. *Exp Neurol* **283**: 110-120.

Yamada N, Hasegawa Y, Yue M, Hamada T, Nakagawa S, Ogawa Y. 2015. Xist Exon 7 Contributes to the Stable Localization of Xist RNA on the Inactive X-Chromosome. *PLoS Genet* **11**: e1005430.

Yildirim E, Kirby JE, Brown DE, Mercier FE, Sadreyev RI, Scadden DT, Lee JT. 2013. Xist RNA is a potent suppressor of hematologic cancer in mice. *Cell* **152**: 727-742.

Zhang LF, Huynh KD, Lee JT. 2007. Perinucleolar targeting of the inactive X during S phase: evidence for a role in the maintenance of silencing. *Cell* **129**: 693-706.

Figure Legends

Figure 1 CIZ1 is enriched at the inactive X chromosome. A) Schematic of CIZ1 indicating replication domain (Copeland et al. 2015), with nuclear localization signal (NLS, green), functional CDK phosphorylation sites (pink), and RXL cyclin-binding motifs (grey); and NM anchor domain (Ainscough et al. 2007) with location of C2H2 type Zn fingers (green); matrin 3-type RNA-binding Zn finger (Prosite PS50171), and acidic domain (E). The location of epitopes recognized by N-term and C-term antibodies are indicated. B) Immunodetection of CIZ1 (green) in female primary embryonic fibroblasts (PEFs) from WT mice, using N- and C-term antibodies. Colocalisation of CIZ1 and histone H3K27me3 (red) was observed in all cells with H3K27me3 staining, as a discrete domain (n>100). DNA is stained with dapi (blue). Additional cell lines are in Figure S1; some have two domains indicative of chromosomal duplication. C) RNA-FISH for *Xist* (red) in female PEFs, showing co-localization with CIZ1 protein (green), and Barr body (grey). Bar is 5μM. D) CIZ1 recruitment to Xi in differentiating XX ESCs correlates with *Xist*-mediated deposition of H3K27me3. d3 and d9 are days of differentiation after withdrawal of LIF. Additional time points are shown in Fig S1C. E) CIZ1 and H3K27me3 in differentiated XX ES cells during mitosis, showing reduction of CIZ1 in late metaphase and complete loss in anaphase but retention of H3K27me3. Bar is 5μm.

Figure 2 CIZ1 is part of the RNA-dependent NM at Xi. A) Maximum intensity projection SR 3D-SIM image of a single C127I cell nucleus, showing adjacent localization of *Xist* foci (green) with CIZ1 foci (red) at the Xi. Examples of individual Z sections from several cells are in Fig S2. B) Schematic showing protocol for serial

extraction with detergent, high-salt, DNase, or RNase, to reveal the protein-RNA nuclear matrix (NM) fraction, or the RNA-independent NM fraction (protein only). C) Images show CIZ1 (red) after serial extraction of 3T3 cells. The proportion of cells with discrete CIZ1-Xi domains is indicated (n>100 for each condition), some with two domains indicating duplication of Xi. Similar results were obtained with PEFs, and are shown in Fig S2C. DNA (blue) shows the extent of nuclease treatment. Images are equally modified to allow direct comparison of fluorescence intensity across the different extraction conditions. Bar is 5μm. D) As in C, but with prior protein-protein cross-linking with DTSP. E) Model showing two populations of CIZ1 in the nuclear matrix (blue); RNA-dependent CIZ1 interacts with *Xist*, RNA-independent CIZ1 is part of the core NM. SAF-A (Hasegawa et al. 2010) is also shown interacting with *Xist* E-repeats, and depicted with YY1 in the RNA-dependent NM.

Figure 3 Delineation of *Xist* and CIZ1 domains. A) Recruitment of the indicated GFP-tagged CIZ1 constructs (Coverley et al. 2005), 24 hours after transient transfection into cycling WT PEFs. The proportion of transfected cells with nuclear GFP, in which accumulation at Xi was observed (n>100 for each construct) is indicated, with representative images. For GFP-C275 endogenous CIZ1 (red) is also shown, detected via epitopes in the N-terminal end. B) Accumulation of GFP-C275 but not GFP-N572 at Xi in a stably expressing ESC line that also carries inducible Xist RNA tagged with Bgl stem loops that bind a BglG-mCherry fusion protein (Moindrot et al. 2015). Almost all (58/61) *Xist*-mCherry expressing cells were positive for GFP-C275, while none (n=47) were positive for GFP-N572. C) Schematic of inducible *Xist* constructs transfected into XY ES cells to study CIZ1 recruitment. The result of CIZ1 localisation studies in the

transgenic cell lines is summarised. D) Example images showing lack of CIZ1 colocalisation with H3K27me3 domains (bottom) or *Xist* (top) in ΔBsPs *Xist* construct missing the E repeat. Absence of *Xist* D repeat (ΔNS) does not affect recruitment of CIZ1. Data for all transgenes is shown in Fig S5.

Figure 4 Expression of X-linked genes. A) Scatter plot showing mean expression in three WT PEF and three CIZ1 null PEF lines (log_2FPKM), for all expressed X-linked transcription units. FPKM below 0.99 were rounded to 1. Mean expression for all X-linked transcription units is in data set S1. B) Heat map showing (white to brown) expression levels in Log_2 FPKM for 62 X-linked genes that are significantly changed in CIZ1 null PEFs ($P< 0.05$). Genes are listed in order against a schematic of the X-chromosome. Unannotated transcripts are indicated by XLOC gene ID number (data set S1), and predicted genes by the prefix Gm. A list of significantly changed transcription units is in data set S2, of which 35 are annotated and 23 have known functions. Right, fold change showing the 34 down-regulated (red) and 28 up-regulated transcription units (green), distributed across the chromosome. Also shown (left of X-chromosome schematic) are results for genes at the XIC. C) Expression of 6 X-linked transcription units where $q<0.05$, showing mean FPKM for three WT and three CIZ1 null cell lines, as well as the effect of re-induction of CIZ1 in null-derived transgenic primary PEF line e13.17.

Figure 5 CIZ1 null mice develop normally but show gross lymphoid abnormalities in adult females. A) *Ciz1*-/- embryos are indistinguishable from WT littermates at E15. B) Growth profiles of *Ciz1*+/+ (n=5) and *Ciz1*-/- (n=8) mice between day 20 and 160 after birth, and C) at 15-18 months old in *Ciz1*+/+ (n=8) and *Ciz1*-/- (n=7) females. No

significant differences were detected. However, *Ciz1*-/- females had enlarged spleen (n=8+/+, 6-/-), liver (n=6+/+, 4-/-) and lung (n=5+/+, 5-/-). Other organs including kidney and heart were not affected. D) Representative image of gross spleen enlargement in *Ciz1*-/- females and with histological sections stained with haematoxylin and eosin (H&E). Lymphoid cell nuclei (stain darkly) are highly organized into foci in *Ciz1*+/+ spleen but not in *Ciz1*-/- spleen. High magnification images (right) show morphology consistent with lympho-proliferative disorder in *Ciz1*-/- mice. Below, immunohistochemical detection of CD20 and CD3 (B and T cell specific, respectively) suggests B-cell lymphoma with T-cell infiltration. Positive cells are stained dark grey, with overlapping distribution. Bar is 200μm. E) Representative H&E staining of *Ciz1*+/+ and *Ciz1*-/- female lymph node, liver and lung. Enlargement of secondary lymphoid tissues in *Ciz1*-/- females correlates with excess proliferation of lymphoid cells as in D. Examples of gross tissue anatomy in *Ciz1*-/- females (right), showing areas of lympho-proliferative disorder as pale outgrowths. Bar is 200μm.

Figure 6 Loss and reinstatement of *Xist* localisation at Xi is dependent on CIZ1. A) Left, immuno-FISH showing CIZ1 and Xist RNA, which is delocalized in CIZ null (-/-) PEFs. DNA is stained with dapi (blue). Quantitation of the area of *Xist* FISH signal is below showing mean distribution over approximately 40% of the nucleus in CIZ1 null PEFs, compared to less than 5% in WT cells. Right, CIZ1 and H3K27me3 in WT and CIZ1 null cells, showing the proportion of cells with marked Xis (n=100). B) X-chromosome paint shows no change in X chromosome territory in CIZ1 null PEFs. C) Double transgenic female PEFs were derived from embryos harbouring a tetracycline responsive *Ciz1* responder transgene and reverse transactivator transgene on the CIZ1

null background. D) *Ciz1* transcript (primers Mm00503766_m1), and E) protein (N-term antibody in whole cell lysates) is detected after doxycycline induction. F) Representative field view of GFP-CIZ1 expressed from the transgene on CIZ1 null background, 24 hours after induction with doxycycline. Note the presence of two domains in some cells indicating duplication of the Xi. Bar is 10um. G) Expression of full length CIZ1 in -/- PEFs leads to relocalisation of *Xist* to Xi. H) Quantitation of the proportion of cells with *Xist* FISH signal that is 'dispersed' (defined as occupation of >10% of the nuclear area). CIZ1 transgene induction reverts CIZ1 null cells to apparent normality for this criterium by 20 hours.

Figure 7 CIZ1 modulates *Xist* localisation in splenocytes A) CIZ1 localisation in WT splenocytes before and after activation with LPS or αCD3. Stimulation causes accumulation of CIZ1 at the Xi in both B and T lymphocytes within 24 hours. Bar is 10μm. B) Xist RNA localisation in splenocytes before and after activation with LPS or αCD3. As for CIZ1, stimulation causes accumulation of *Xist* at the Xi of WT B and T lymphocytes within 24 hours, whereas Xist RNA is not properly localised in CIZ1 null cells. Bar is 10μm. n=200-300/group.

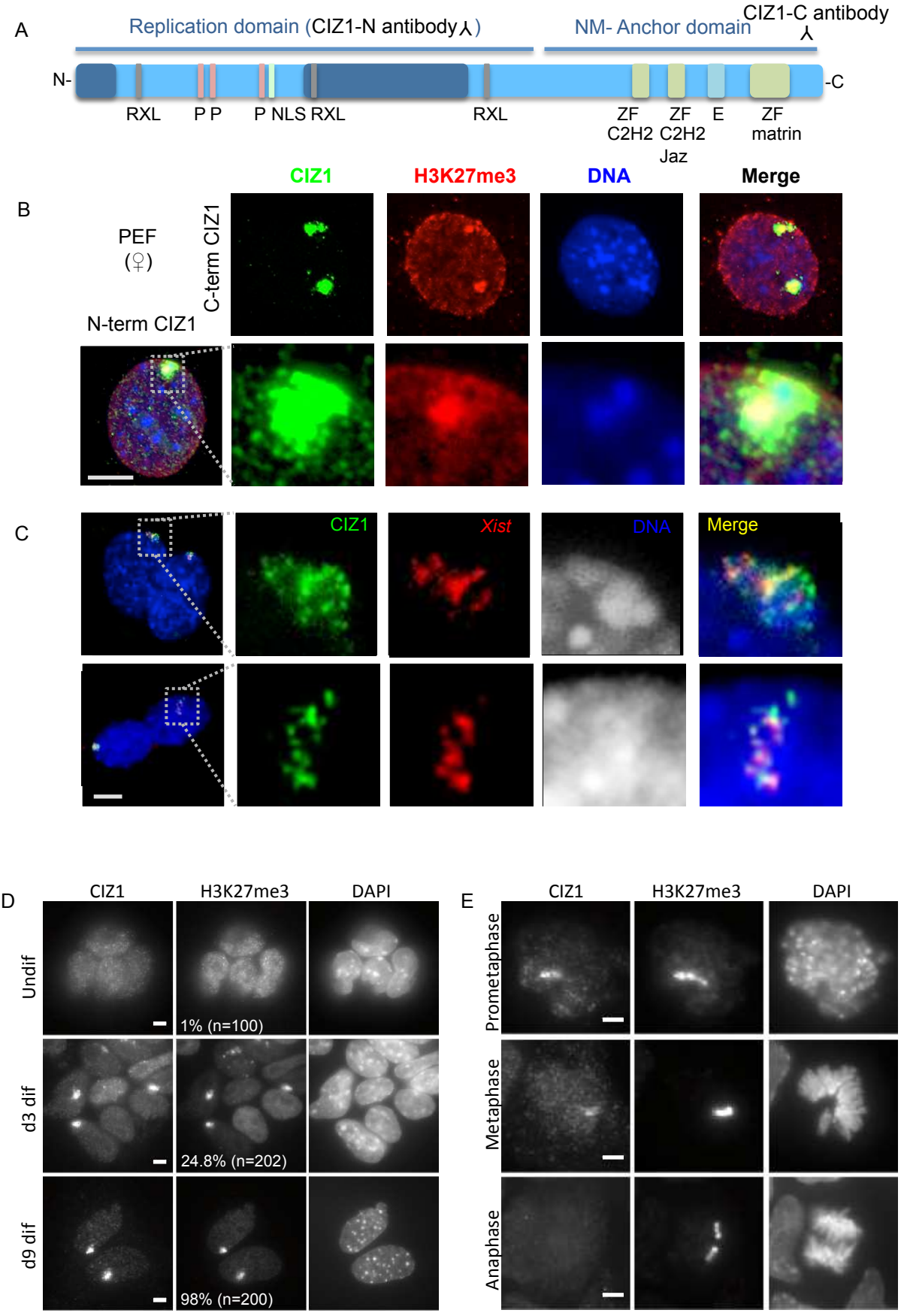
A
Replication domain (CIZ1-N antibody人)
NM- Anchor domain
CIZ1-C antibody人
N-
-C
RXL
P P
P NLS RXL
RXL
ZF C2H2
ZF C2H2 Jaz
E
ZF matrin
B
CIZ1
H3K27me3
DNA
Merge
PEF (♀)
C-term CIZ1
N-term CIZ1
C
CIZ1
Xist
DNA
Merge
D
CIZ1
H3K27me3
DAPI
Undif
1% (n=100)
d3 dif
24.8% (n=202)
d9 dif
98% (n=200)
E
CIZ1
H3K27me3
DAPI
Prometaphase
Metaphase
Anaphase

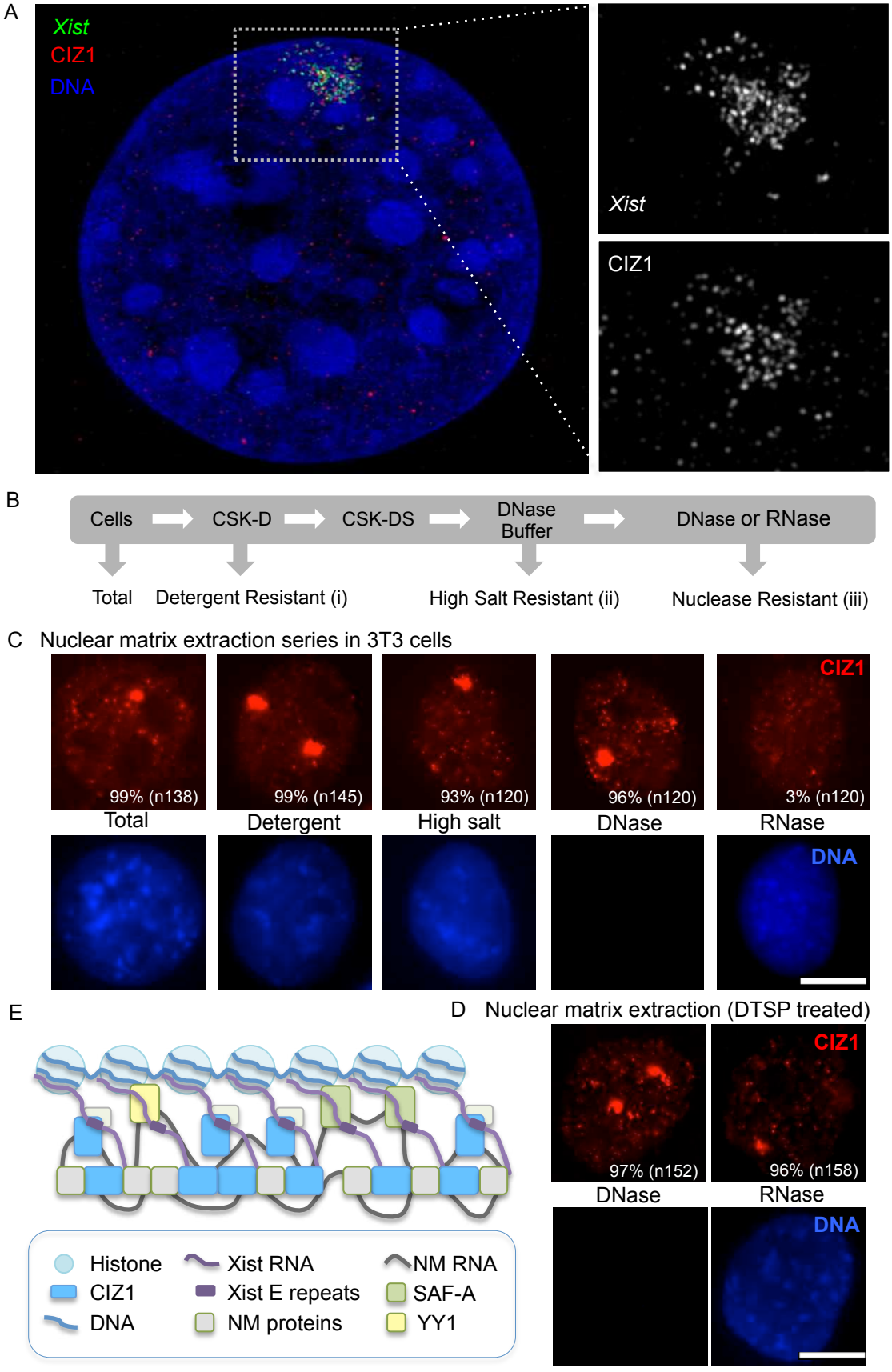
A
Xist
CIZ1
DNA
Xist
CIZ1
B
Cells
CSK-D
CSK-DS
DNase Buffer
DNase or RNase
Total
Detergent Resistant (i)
High Salt Resistant (ii)
Nuclease Resistant (iii)
C Nuclear matrix extraction series in 3T3 cells
99% (n138)
99% (n145)
93% (n120)
96% (n120)
3% (n120)
CIZ1
Total
Detergent
High salt
DNase
RNase
DNA
E
D Nuclear matrix extraction (DTSP treated)
97% (n152)
96% (n158)
CIZ1
DNase
RNase
DNA
Histone
CIZ1
DNA
Xist RNA
Xist E repeats
NM proteins
NM RNA
SAF-A
YY1

A

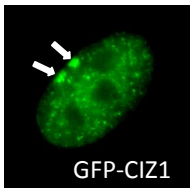

GFP-CIZ1 81 %
GFP-N572 0 %
GFP-C275 14 %

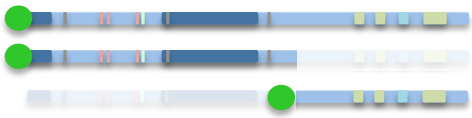

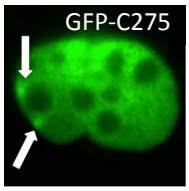

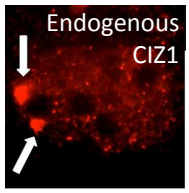

B

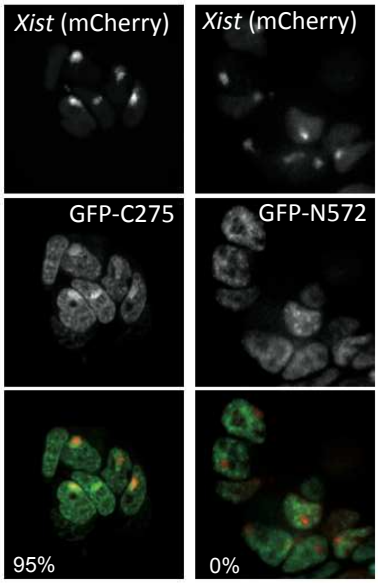

C

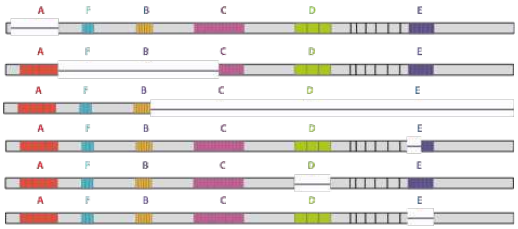

% of cells with CIZ1 enriched *Xist* domains

90 +/- 7.1
98 +/- 3.5
0 +/- 0
72 +/- 5.2
99 +/- 1.4
0 +/- 0

D

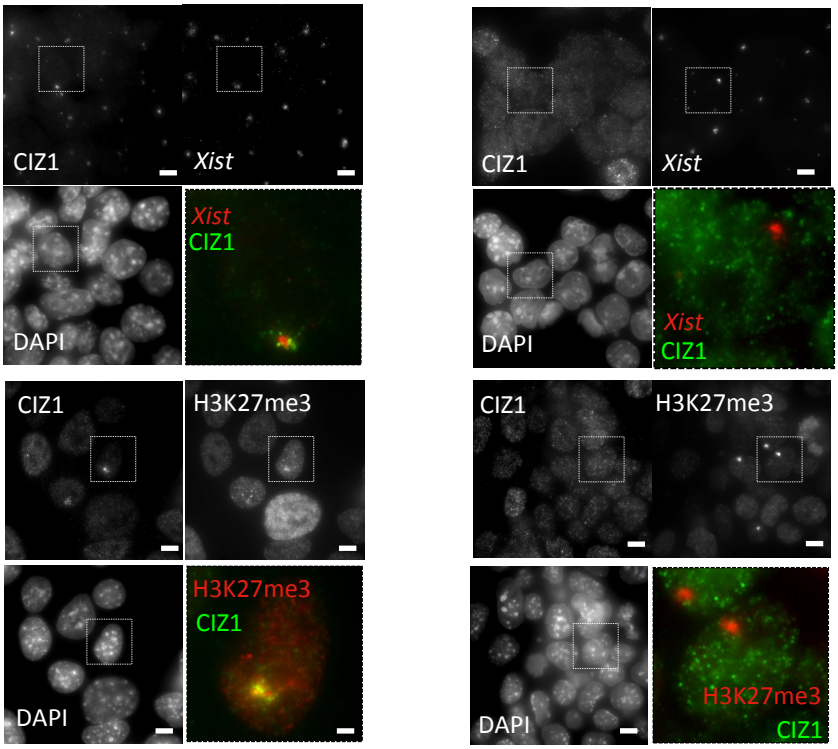

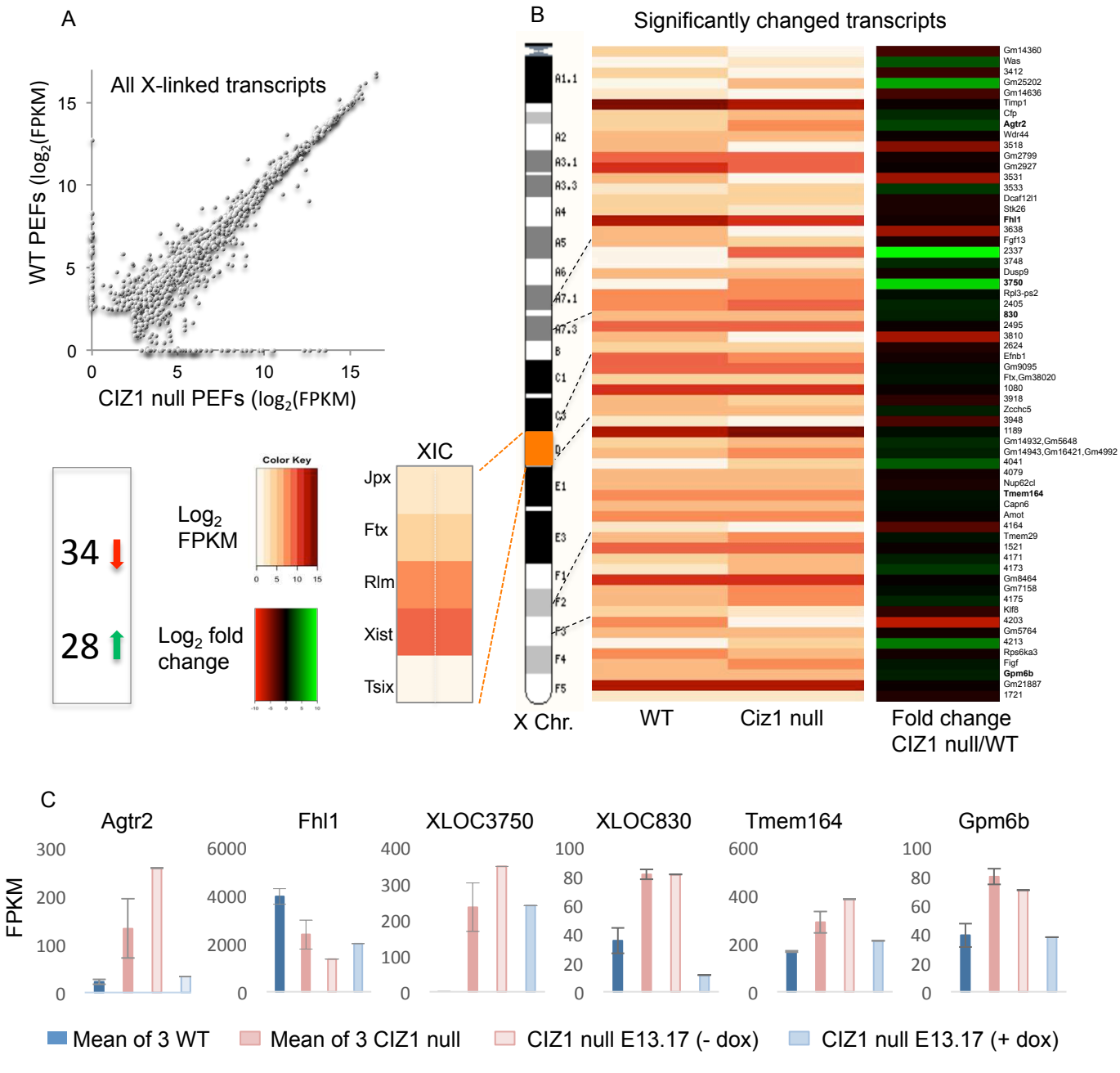
A
All X-linked transcripts
WT PEFs (log2(FPKM)
CIZ1 null PEFs (log2(FPKM)
0
5
10
15
34
28
Log2 FPKM
Color Key
Log2 fold change
XIC
Jpx
Ftx
Rlm
Xist
Tsix
B
Significantly changed transcripts
X Chr.
WT
Ciz1 null
Fold change CIZ1 null/WT
Gm14360
Was
3412
Gm25202
Gm14636
Timp1
Cfp
Agtr2
Wdr44
3518
Gm2799
Gm2927
3531
3533
Dcaf12l1
Stk26
Fhl1
3638
Fgf13
2337
3748
Dusp9
3750
Rpl3-ps2
2405
830
2495
3810
2624
Efnb1
Gm9095
Ftx,Gm38020
1080
3918
Zcchc5
3948
1189
Gm14932,Gm5648
Gm14943,Gm16421,Gm4992
4041
4079
Nup62cl
Tmem164
Capn6
Amot
4164
Tmem29
1521
4171
4173
Gm8464
Gm7158
4175
Klf8
4203
Gm5764
4213
Rps6ka3
Figf
Gpm6b
Gm21887
1721
C
Agtr2
Fhl1
XLOC3750
XLOC830
Tmem164
Gpm6b
FPKM
Mean of 3 WT
Mean of 3 CIZ1 null
CIZ1 null E13.17 (- dox)
CIZ1 null E13.17 (+ dox)

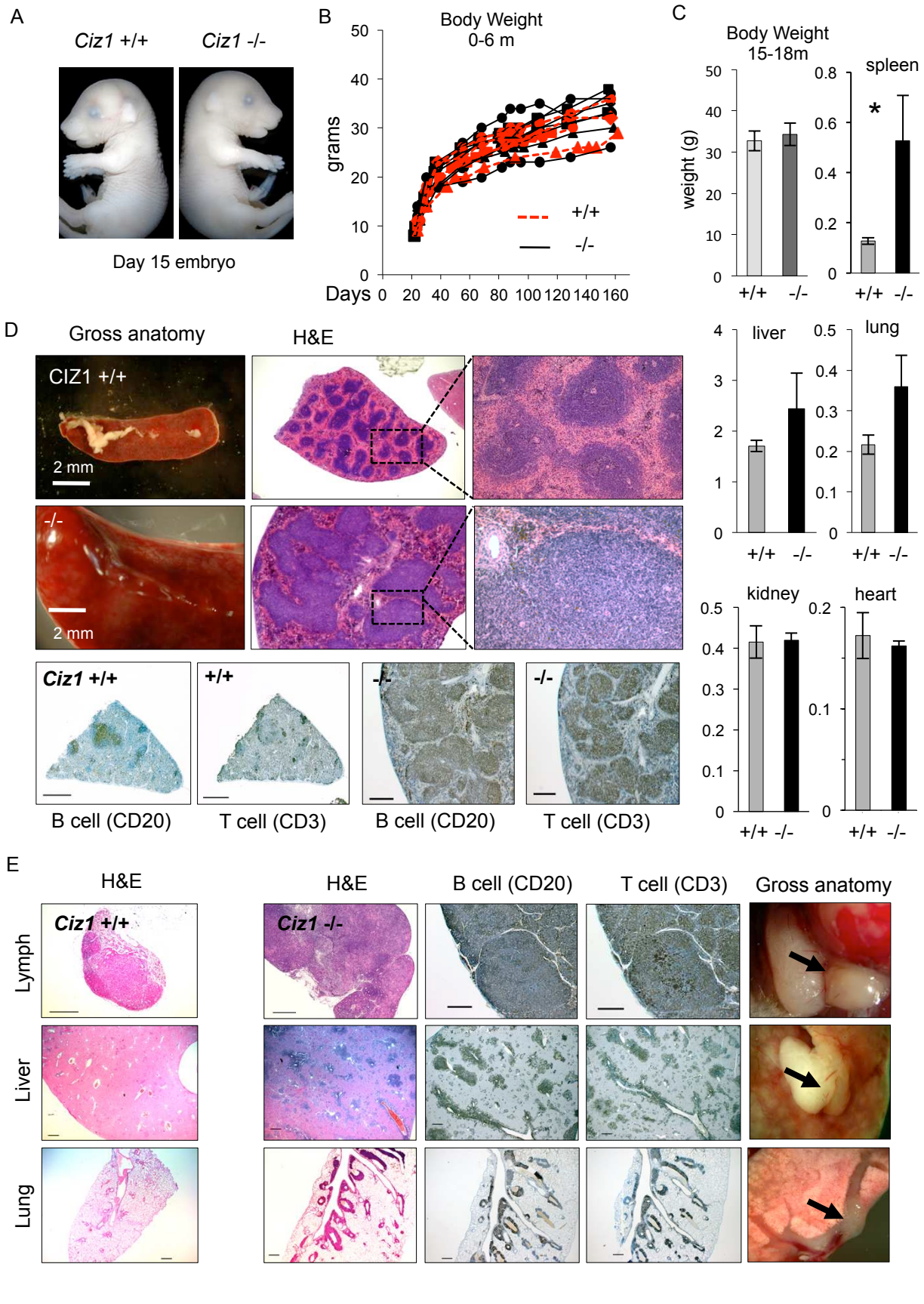
A
Ciz1 +/+
Ciz1 -/-
Day 15 embryo
B
Body Weight
0-6 m
grams
Days
+/+
-/-
C
Body Weight
15-18m
weight (g)
spleen
*
+/+ -/-
D
Gross anatomy
H&E
CIZ1 +/+
2 mm
-/-
2 mm
liver
lung
kidney
heart
Ciz1 +/+
+/+
-/-
-/-
B cell (CD20)
T cell (CD3)
B cell (CD20)
T cell (CD3)
E
H&E
H&E
B cell (CD20)
T cell (CD3)
Gross anatomy
Lymph
Liver
Lung
Ciz1 +/+
Ciz1 -/-

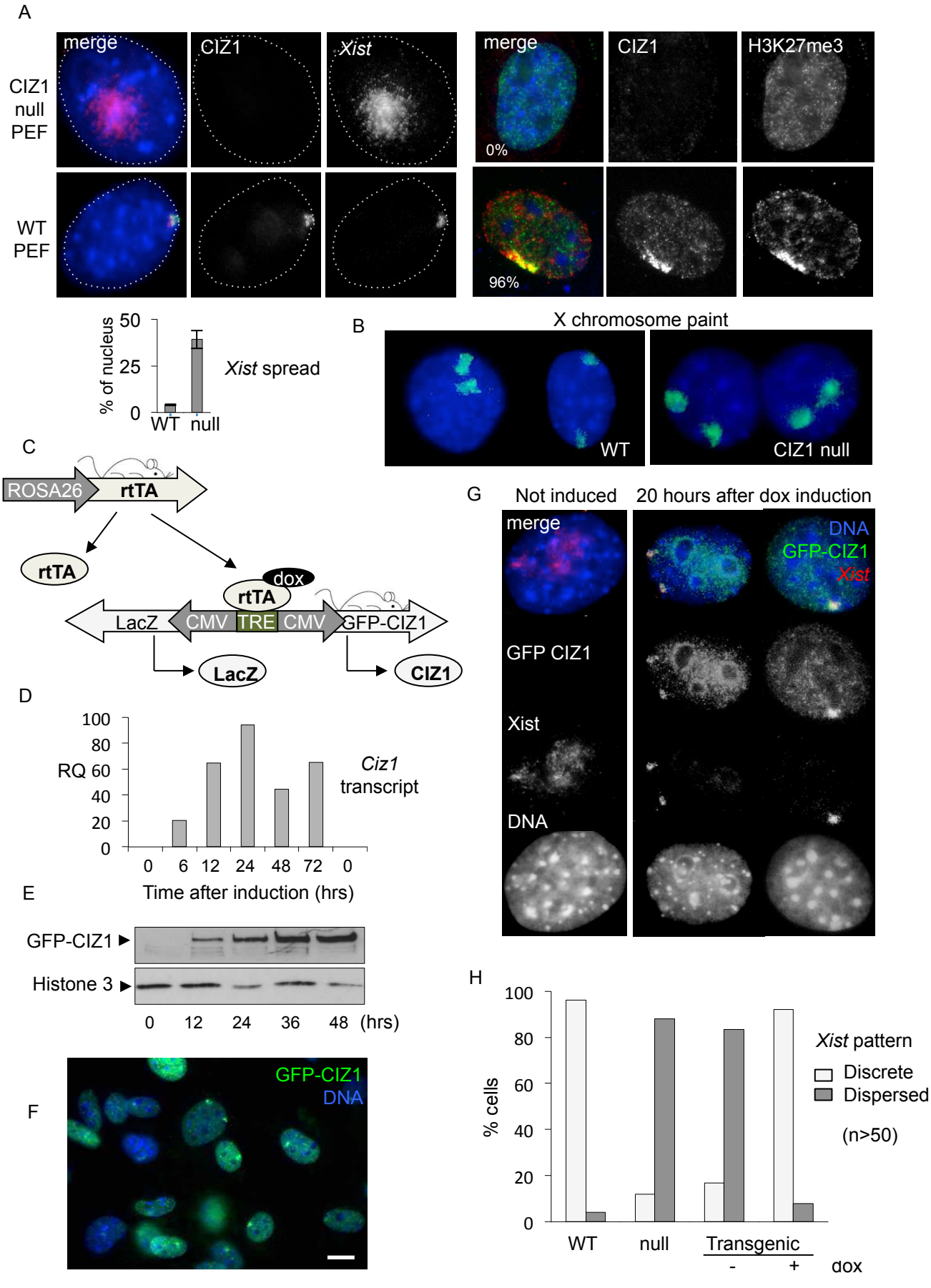
A
CIZ1 null PEF
WT PEF
merge
CIZ1
Xist
H3K27me3
0%
96%
% of nucleus
50
25
0
WT
null
Xist spread
B
X chromosome paint
WT
CIZ1 null
C
ROSA26
rtTA
rtTA
dox
rtTA
LacZ
CMV
TRE
CMV
GFP-CIZ1
LacZ
CIZ1
D
RQ
100
80
60
40
20
0
Ciz1 transcript
0 6 12 24 48 72 0
Time after induction (hrs)
E
GFP-CIZ1
Histone 3
0 12 24 36 48 (hrs)
F
GFP-CIZ1
DNA
G
Not induced
20 hours after dox induction
merge
GFP CIZ1
Xist
DNA
DNA
GFP-CIZ1
Xist
H
% cells
100
80
60
40
20
0
WT
null
Transgenic
-
+
dox
Xist pattern
Discrete
Dispersed
(n>50)

A CIZ1 localisation in mouse splenocytes

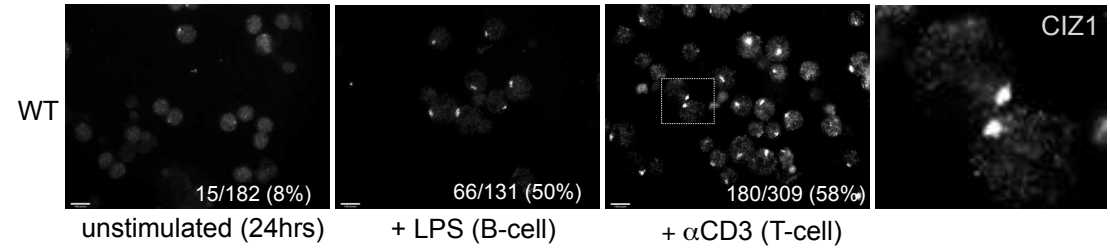

B *Xist* localisation in mouse splenocytes

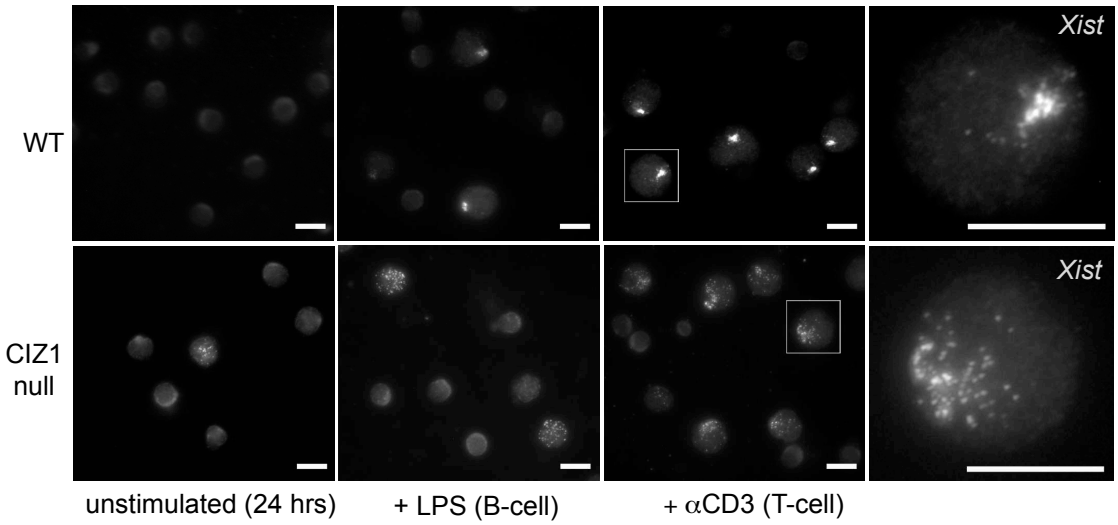

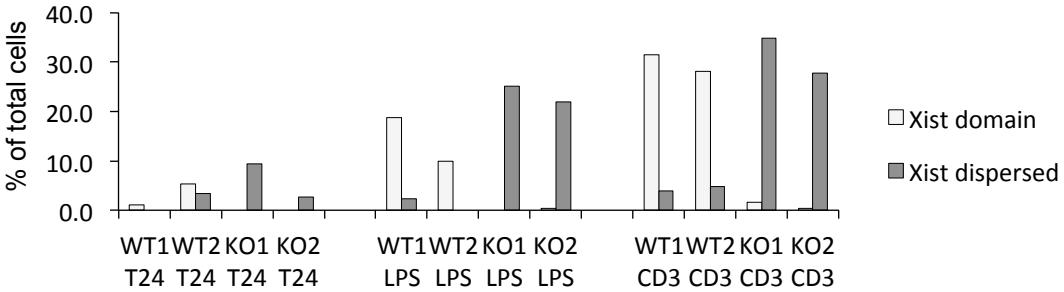

Supplemental Materials and Methods

Animals and genotyping All animal work was carried out with ethical approval from the University of Leeds, UK, where the animals were maintained under specific pathogen free conditions. CIZ1 null mice were generated from *Ciz1*+/- C57BL/6 embryonic stem (ES) cell clone IST13830B6 (Texas A&M Institute for Genomic Medicine) harboring a neomycin resistance gene trap insertion into intervening sequence (IVS) 1. Heterozygous mice were mated to produce homozygous progeny and identified by genotyping of ear biopsies (live born mice) or yolk sac (embryos). Absence of CIZ1 was confirmed for mRNA and protein, using qPCR, immunofluorescence and immunoblot. *GFPCiz1*-Tg mice, harbouring an inducible GFP-full length mouse *Ciz1* construct (Bageghni et al. 2016), were crossed with ROSA26-rtTA mice (B6.Cg-Gt(ROSA)26Sortm1(rtTA*M2)Jae/J; Jackson laboratories) to enable inducible expression of *GFPCiz1* in a wide range of cell types. Thus, double transgenic mice harboured a responder transgene with regulatable GFP tagged full-length mouse *Ciz1* and a LacZ reporter under control of a bidirectional minimal CMV promoter, and an activator transgene encoding reverse-tetracycline regulatable trans-activator (rtTA) under control of the ubiquitous ROSA26 promoter. Production of GFP-CIZ1 was only induced upon exposure to doxycycline. All samples were lysed overnight in tissue lysis buffer (1% SDS, 10mM TRIS pH 7.4, 50mM EDTA, 100 μg/ml proteinase K), and DNA isolated under standard conditions. Purified DNA was subjected to PCR genotyping using primer IVS1F in combination with IVS1R to detect the wild type *Ciz1* +/+ allele, IVS1F and VR to detect the *Ciz1*-/- targeted allele, tTA1 and tTA2 to detect transactivator, LZ4 and LZ5 to detect LacZ, and for sex identification of embryos Sry1 with Sry2, using the following conditions: 94ºC (5 min), 60ºC (30 sec), 72ºC (45 sec), followed by 29 cycles of 94ºC (15 sec), 60ºC (30 sec), 72ºC (45 sec), and extension at 72ºC (7 min). Primers used for characterisation of *Ciz1* targeting and for detection of transactivator and responder transgenes, and sex, are shown below.

Gene	Forward primer	Reverse primer	Size
Ciz1 +/+	IVS1F: GTGGCGTTGGCTATATCTGC	IVS1R: GTTGAACATGGTGGCTGAAG	515 bp
Ciz1 -/-	IVS1F: GTGGCGTTGGCTATATCTGC	VR: CCAATAAACCCTCTTGCAGTTGC	360 bp
rtTA	tTA1: CGCTGGGGGGCATTTTACTTTA	tTA2: CATGTCCAGATCGAAATCGTC	450 bp
LacZ	LZ4: AATGGTCTGCTGCTGCTGAACG	LZ5: GGCTTCATCCACCACATACAGG	225 bp
Sry	Sry1: TGTCTAGAGAGCATGGAGGG	Sry2: TGTGACACTTTAGCCCTCCG	263 bp

Mouse Primary Embryonic and Tail Tip Fibroblasts (PEFs/TTFs), and other cell lines For PEFs embryos were retrieved at day 13 or 14 of gestation and dissected in ice-cold sterile PBS to remove head and visceral organs. The carcass was disrupted by repeated passage through an 18G needle in culture media (DMEM containing 10% foetal calf serum (PAAgold), 100u/ml Penicillin, 10 μg/ml Streptomycin, 2 mM L-glutamine). Each embryo was prepared into a single 2ml well, and the cells allowed to settle for 16-24 hours at 37ºC, 5% CO_2, before residual tissue was removed by repeated washing with PBS and replaced with 2ml fresh culture media. Attached cells proliferated to form colonies within 2 days, which were passaged once by splitting 1/5 to form a uniform monolayer prior to freezing (P1 cells). For TTFs approximately 1cm of tail tip from 3-week old mice was surface sterilized by brief dipping in 70% ethanol, skin removed, and transferred into ice cold PBS. Under sterile conditions the tissue was cut into fragments in 1ml culture media. After 4-7 days incubation, tissue fragments were removed as for PEFs. The

cells were passaged 1/3 at high density and cultured to form a monolayer prior to freezing at P2. Confirmation of cell line genotype and sex was performed after explant culture, using primers shown above. For inducible cells harbouring transactivator and responder transgenes addition of doxycycline to media (5-10 μg/ml) was used to induce detectable GFP-CIZ1 within 6 hours. Female 3T3 cells were grown as described (Coverley et al. 2002) in DMEM (Sigma), 1% Penicillin, streptomycin, glutamine (Gibco),10% FBS. ES cells were grown on feeders (Puromycin resistant SNL) at 37°C 5% CO2 in DMEM (Life Technologies) supplemented with 10% fetal calf serum (Seralab), 2mM L-Glutamine (Life Technologies), 1X non-essential amino-acids (Life Technologies), 50μM 2-mercaptoethanol (Life Technologies), 1X Penicillin-Streptomycin (Life Technologies) and LIF-conditioned medium, made in-house, at a concentration equivalent to 1000 U/ml. To induce *Xist* expression, ES medium was supplemented with 1.5μg/ml doxycycline. C127I cells were grown at 37°C 5% CO2 in DMEM supplemented with 10% fetal calf serum, 2mM L-Glutamine, 1X non-essential amino-acids, 50μM 2-mercaptoethanol, 1X Penicillin-Streptomycin. All other cells were from ECACC or JCRB and cultured as recommended. Details of all cells used are given below.

Cell Lines S numbers refer to RNAseq sample numbers.

Name	**Sex**	**Type**	***Ciz1***	**Ref.**
e13.1 (S10)	Female	Primary embryonic fibroblast	+/+	This study.
e13.8 (S11)	Female	Primary embryonic fibroblast	+/+	This study.
e14.4 (S9)	Female	Primary embryonic fibroblast	+/+	This study.
e13.15 (S13/15)	Female	Primary embryonic fibroblast	-/-	This study.
e14.2 (S12)	Female	Primary embryonic fibroblast	-/-	This study.
E13.17 (S14/16)	Female	Primary embryonic fibroblast	-/- with inducible full length *Ciz1* transgene	This study.
E13.2 (S17)	Male	Primary embryonic fibroblast	+/+	This study.
E13.6 (S18)	Male	Primary embryonic fibroblasts	-/-	This study.
1016	Female	Immortalised tail tip fibroblast cell line	-/-	This study.
E13.17 stable	Female	Culture immortalised PEF-derived stable line	-/- with inducible full length *Ciz1* transgene	This study.
MG-3E	Male	XY murine Embryonic stem cell line with inducible *Xist*	+/+	(Moindrot et al. 2015)
P4D7	Male	XY murine Embryonic stem cell line	+/+	(Moindrot et al. 2015)
P4D7F4	Male	XY murine Embryonic stem cell line with mCherry *Xist*	+/+	(Moindrot et al. 2015)
PGK12.1	Female	XX murine Embryonic stem cell line	+/+	(Penny et al. 1996)
C127I	Female	XX mouse mammary epithelial cell line	+/+	(Lowy et al., 1978)
3T3	Female	Immortalized murine fibroblast	+/+	(Coverley et al. 2002)
TIG1	Female	Human stable fetal lung	+/+	(Aizawa et al.

				1980)
WI38	Female	Human stable fetal lung	+/+	(Hayflick and Moorhead 1961)
MCF10A	Female	Human breast epithelial cell line	+/+	(Soule et al. 1990)
MCF7	Female	Human breast epithelial cancer cell line	n/d	(Soule et al. 1973)

Quantitative RT-PCR RNA was isolated from embryos, PEFs, TTFs and tissues using TRIzol (Ambion), reverse transcribed to cDNA with SuperScript III (Invitrogen) using random hexamers (Sigma). cDNA was analysed using gene specific primers and probes and expression calculated using the formula 2^{-dCT}, and expressed relative to controls. Primer-probe sets (Applied Biosystems) used for quantitative investigation of gene expression are shown below.

Gene	Exon	Assay	Product Size (bp)
Ciz1	10-11	Mm00503766_m1	77
GapdH	2-3	Mm99999915_g1	107
Xist	1-2	Mm01232884_m1	65
Hprt	2-3	Mm01545399_m1	81

Transcriptome analysis PEF cell lines E13.1, E13.8 and E14.4 (all female WT), E13.15, E13.17 and E14.2 (all female *Ciz1* null), E13.2 (male WT) and E13.6 (male *Ciz1* null), all at passage 4, were grown to 80% density and RNA extracted with TRIzol (Ambion 15596-026) following manufacturer's instructions, then treated with DNase (Roche 04716728001), before quality analysis by agarose gel, NanoDrop spectrophotometer and Agilent 2100 Bioanalyzer. Libraries were prepared with NEBNext® Ultra™ RNA library Prep Kit for Illumina®, and enriched for mRNA using NEBNext Poly(A) mRNA Magnetic Isolation Module, which is optimized for production of libraries with 250-400 bp inserts. Enriched mRNA was fragmented by sonication, random priming cDNA, synthesis, end repair, dA-tailing, adaptor ligation and PCR enrichment. Libraries were sequenced at the Leeds Institute for Molecular Medicine (LIMM) using Illumina 3000 system, using paired-end sequencing to generate ~50 million reads per sample. Further information on the cell lines used is given in Supplemental Table- Cell Lines.

Bioinformatics STAR software (Dobin et al. 2013) was used for alignment of sequencing reads to the X chromosome of the C57BL/6 mouse (Mus_musculus GRCm38 primary assembly, downloaded from Ensembl.org [Access date: 4/05/2016]). Cufflinks was used for transcriptome assembly of the mapped reads (Trapnell et al. 2010; Roberts et al. 2011) followed by differential expression analysis with Cuffdiff (Trapnell et al. 2013) which provided quantified levels of expression. Initial filtering involved exclusion of transcriptional units with "no test" or "fail" test status, which indicate that no statistical test could be performed and no p-value calculated, followed by selection of transcription units with a p-value equal to or less than 0.05 (85 transcription units). This was followed by manual exclusion of those with no gene expression for all but one of the samples, rendering a total of 62 from the X chromosome, 27 of which correspond to non-annotated open reading frames and therefore possible novel-transcripts, referred to here by their Cufflinks XLOC number (refer to supplemental Xl files for ensemble locus identifiers). Heat maps were generated using R software (R Core Team 2016 https://www.R-project.org/,) using the gplots package (Warnes et al, 2016 https://CRAN.R-project.org/package=gplots) and RColorBrewer (Neuwirth, 2014 https://CRAN.R-project.org/package=RColorBrewer). Gene enrichment analysis was carried out with GSEA software (Mootha et al. 2003; Subramanian et al. 2005). In the mouse approximately 3.3% of genes escape XCI and remain transcriptionally active, (Yang et al. 2010), many of which are thought to have female-specific functions that contribute to sexual dimorphism (Berletch et al. 2011). The subset that escape silencing vary between cell type and developmental stage (Gendrel et al. 2012), with some genes (constitutive escapees) avoiding silencing in most cell types, and others (facultative escapees) only in specific contexts. Direct comparison with the subset of 23 translated X-linked genes with known function that are significantly affected by loss of CIZ1, revealed no significant overlap

with constitutive escapees, but five genes (*Cfp, Ftx, Tmem164, Tmem29, Gpm6b*) are facultative escapees in specific mouse tissues (Berletch et al. 2011). *Cfp* escapes X inactivation in the spleen (Maves and Weiler 1992) and is also significantly upregulated upon knockdown of *Xist* in the blood compartment of mice (Yildirim et al. 2013), while *Tmem164* is affected by knockdown of both *Xist* (Yildirim et al. 2013) and *Smchd1* (Gendrel et al. 2013).

Histology Tissues were dissected from mice into ice cold PBS, washed twice, blotted dry, then weighed. Representative tissues were photographed using a Nikon D70S digital camera attached to a Zeiss SV6 dissecting microscope. Tissues were divided into two, one half put immediately into histological grade formalin and the rest snap frozen in nitrogen and stored at -80ºC. After 24-48 hrs the formalin was replaced with 70% ethanol and the tissues processed for histology by embedding in paraffin. Dewaxing and antigen retrieval were performed in a Menarini Retrieval unit (Menarini diagnostics) and sections processed using an Intellipath autostainer.

ES cell differentiation PGK12.1 XX ES cells (Penny et al. 1996) were grown in ES media (DMEM, 10% FCS, non-essential amino acids (Invitrogen), 2mM L-glutamine, 0.05mM b-mercaptoethanol, pen/strep (Invitrogen) with LIF on gelatinised tissue culture dishes without feeders. To induce differentiation ES cells were trypsinised, resuspended in the same media without LIF, and re-plated at a density of $1x10^6$ cells/90mm non-gelatinised tissue culture dish. The media was replaced on days 2 and 3, then the differentiating colonies were gently detached and replated onto bacterial culture dishes to stimulate embryoid body formation. The media was replaced daily for the next 3 days. On day 7 the embryoid bodies were transferred to non-gelatinised tissue culture dishes to reattach. Fibroblast outgrowths were passaged as required after day 8. To analyse CIZ1 localisation in ES cells after induction of *Xist*-Bgl-mCherry expression, CIZ1 C-terminal anchor domain (C275) and the N-terminal DNA replication domain (N572) sequences were PCR amplified and inserted into pCAG-GFP-IRES-puro eukaryotic expression vector using ligation independent cloning (LIC). 2µg of each plasmid was lipofected into P4D7F4 ES cell line and puromycin-resistant colonies were picked and characterised. *Xist* expression was induced in CIZ1-GFP positive clones by addition of doxycycline (2µg/ml). Cells were imaged 24 hrs later on PE Ultraview spinning disk confocal microscope.

Nuclear Matrix extraction Cells were serially extracted as previously described (Wilson et al. 2016), and are referred to by the most aggressive treatment given. Coverslips were treated with CSK 10mM PIPES/KOH pH6.8, 100mM NaCl, 300mM Sucrose, 1mM EGTA, 1mM MgCl2, 1mM DTT, 1 cOmplete™ Protease Inhibitor Cocktail per 50mL (11697498001) supplemented with 0.1% Triton-X-100 and made with DEPC water (CSK-D), followed by 0.5M NaCl in CSK-D, a double wash with DNase Buffer (40mM Tris/HCl, 10mM NaCl, 6mM $MgCl_2$, 1mM $CaCl_2$, pH 7.9) and 1 hour incubation at 37°C in DNase Buffer with or without DNase I (Roche 04716728001) or RNase (Roche 11119915001). Coverslips were then washed with 0.5M NaCl in CSK-D before fix in 8% paraformaldehyde. Vanadyl Ribonucleoside Complex (VRC, NEB S1402S) was added at 2.5mM to all buffers with the exception of the coverslips to be treated with RNase, in which VRC was omitted from the digestion step, the previous two wash steps, and the CSK-DS rinse. Fixed coverslips were further processed for immunofluorescence. Where indicated cells were treated with cross-linking agent DTSP as described (Hesketh et al. 2015), prior to extraction.

Western blots and immunofluorescence For western blotting, cells were grown in tissue culture treated plates, washed in ice cold PBS and scraped into Laemmli loading buffer. Samples were separated by 8% SDS-PAGE and transferred to nitrocellulose blots using iBlot system (Invitrogen). Blots were blocked in 5% milk, 1x TBS, 0.1% Tween-20 except for probing with α-CIZ1 (1793, Coverley et al., 2005) when TBS was substituted for PBS. Blots were probed with primary antibodies for 2hr, RT, washed, probed with secondary antibodies for 1hr, RT and washed before developing with EZ-ECL (Biological Industries) and Hyperfilm™ (GE Healthcare). Antibodies used were α-actin mAb (Sigma), α-CIZ1 N-term 1794 pAb (Coverley et al., 2005), with anti-HRP-conjugated goat α-mouse or α-rabbit (Abcam). For immunofluorescence cells were grown on coverslips then washed in PBS and fixed in 4% PFA to reveal total protein, or washed in PBS, washed in 0.1% Triton-X 100 then fixed in 4% PFA to extract soluble proteins and reveal the chromatin/nuclear matrix immobilised fraction (detergent treated). Coverslips were blocked in AB (1x PBS, 10 mg/ml BSA, 0.02% SDS, 0.1% Triton-X 100), for 30 mins then incubated with primary antibodies for 2hrs, 37°C, washed in AB, incubated with secondary antibodies for 1hr, 37°C, washed and mounted on slides. For ES cell differentiation course Pgk12.1 cells were grown on Superfrost Plus glass slides (BDH). Slides were rinsed in PBS and cells were fixed in 2% formaldehyde for 15 min followed by permeabilisation in 0.4% Triton X100 for 5 min. Cells were blocked with fish gelatin (Sigma) and incubated with H3K27Me3 antibody (Active Motif, ab61017) and α-CIZ1 N-Term (1794) for 2 hrs at rt. After incubation with secondary antibody the cells were rinsed with PBS and mounted with Vectashield medium containing DAPI (Vector labs).

RNA-FISH: Female cultured cells (early passage e13.1 +/+, late passage e14.4 +/+ and early passage inducible e13.17 -/- ± dox, and late passage female TTF -/- line 1016) were first processed for detection of *Xist* transcript (red) by RNA-FISH under RNase free conditions, followed by immuno-FISH for CIZ1 (green) using 1794, as detailed below. Briefly, cells grown on coverslips were fixed with 4% PFA on ice for 10 mins, rinsed 3X in PBS, then incubated for 10 mins in PBS supplemented with Triton X-100 (0.5%), BSA (0.5%), vanadyl ribonucleoside complex (VRC, 2mM). An 11 kb Spe1-Sal1 *Xist* fragment (~500ng) isolated from a full length mouse *Xist* clone pCMV-*Xist*-PA (Addgene 26760) was fluorescently tagged using BioPrime labelling kit (Invitrogen 18094-011), replacing the biotin with Cy3-dUTP (GE Healthcare PA53022). Following overnight labelling the reaction was supplemented with Cot1 and salmon sperm DNA to compete for repetitive elements. The mix was repeat precipitated two times and then resuspended in 80ul hybridisation buffer comprising 50% formamide in 2X SSC with BSA (2mg/ml), dextran sulphate (10%) and VRC (10mM). Prior to use the probe (10ul / coverslip) was denatured at 74C for 10 mins, then annealed at 37C for 20 mins. Coverslips were dehydrated through an ethanol series and air-dried. Probe was spotted onto a clean RNase free slide and overlaid with the coverslip, then sealed with rubber cement and incubated overnight at 37C in the dark. Unused labelled probe was stored at -20C. The coverslip was then carefully removed in 4X SSC, washed three times in 2X SSC with 50% formamide at 39C, three times in 2X SSC at 39C, once in 1X SSC at room temperature, then once in 4X SSC at room temperature. All washes were for 5 mins and supplemented with VRC. For detection of CIZ1 signal, coverslips were further washed three times in PBS before incubating in antibody buffer (PBS with BSA (10mg/ml), Triton X-100 (0.1%) and SDS (0.02%) for 20 mins. CIZ1 N-term antibody 1794 (1:1000) was applied for 1 hour, followed by secondary anti-rabbit FITC (Sigma F9887) at 1:500 for 1 hour. After three further PBS washed the coverslips were briefly dipped in water and mounted in vectorshield with dapi, imaged and processed using Adobe Photoshop CS4 to enhance signal definition. Area of nucleus encompassed by *Xist* signal (cloud spread) was determined using the lasso tool in Adobe Photoshop (CS4). For SR-3DSIM RNA-FISH samples were processed as follows: 1μg *Xist* cDNA was labelled with green-dUTP (Abbott Molecular) using a nick translation kit (Abbott Molecular) in a total volume of 50μL. Cells for SR-3DSIM were seeded onto No. 1.5H (170 μm ± 5 μm) coverslips (Marienfield) and if necessary, *Xist* expression was induced with doxycycline. Cells were fixed with 3 % formaldehyde for 10 min, permeabilised in 0.5% Triton X-100 PBS for 10 minutes. Initial blocking (30 min) and all further antibody incubations were carried out in 3% BSA, 5% normal goat serum (Sigma), 0.5% fish gelatine and RNasin (Promega) in PBS with 0.05% tween-20. Coverslips were incubated with primary antibody for 1 h in a humidified chamber (rabbit anti-CIZ1 1794, 1/2000). After extensive washing in PBS-T, coverslips were incubated with Alexa Fluor goat anti-rabbit 594,1/1000 for 30min. Coverslips were again extensively washed, then post fixed with 3 % formaldehyde. Coverslips were then incubated with 10 μl labelled *Xist* probe in FISH hybridisation buffer and incubated overnight in a humidified chamber. The following day, the coverslips were washed 3 times with 50% formamide, 2X SSC at 42°C, and 3 times with 2X SSC at 42°C. Coverslips were then incubed with 2μg / ml DAPI for 10 minutes, briefly washed and mounted using Vectorshield onto slides. (Cobb et al. 2005)

Chromosome paints FITC conjugated X chromosome paints (Cytocell AMP 0XG) were used following the manufacturers' instructions on early passage WT e13.1 and inducible KO e13.17 (± dox) cells. Cells grown on coverslips were immersed in 2X SSC for 2 mins, then dehydrated through an ethanol series and allowed to dry. Both probe and sample were prewarmed to 37C for 5 mins prior to application of 10μl probe. This was overlaid with a coverslip and sealed with rubber glue. The sample was denatured for 2 mins at 75C and incubated overnight in the dark at 37C. The coverslip and glue removed and the sample washed in 0.4X SSC at 72C for 2 mins, then 2X SSC 0,05% Tween for 30 secs, then mounted in vectorshield with dapi and imaged.

Microscopy Super-resolution 3D-SIM image stacks were acquired with a z-distance of 125nm and with 15 raw images per plane (5 phases, 3 angles). The raw data was computationally reconstructed with SoftWoRx 6.1 (GE Healthcare) using channel-specifically measured optical transfer functions (OTFs) and Wiener filter settings 0.0020 (green/red channel) and 0.0040 (blue channel), respectively, to generate 3D stacks with ~120nm lateral and ~300nm axial resolution. Spherical aberration was minimized by matching the refractive indices (RI) of the immersion oil for sample acquisition (RI 1.514) and for generation OTFs (RI 1.512 for the blue and green, and 1.514 for the red OTFs) generated from ~100nm diameter blue (FluoroMax; Thermo Scientific), green and red (FluoSpheres; Life Technologies) beads, respectively. Lateral colour channel alignment was performed using a special image registration slide and algorithm provided by GE Healthcare. Correct 3D alignment was confirmed and refined in z by a custom test sample with two layers of 0.2μm diameter TetraSpeck beads (Life Technologies). The full-scale 32-bit

reconstructed data was thresholded for each channel to the stack modal grey value (representing the centre of the background intensity level) and converted to 16-bit composite tif-stacks using an in-house script in ImageJ (http://rsbweb.nih.gov/ij) before further processing.

Supplemental References

Aizawa S, Mitsui Y, Kurimoto F, Matsuoka K. 1980. Cell-surface changes accompanying aging in human diploid fibroblasts: effects of tissue, donor age and genotype. *Mech Ageing Dev* **13**: 297-307.

Bageghni SA, Frentzou GA, Drinkhill MJ, Mansfield W, Coverley D, Ainscough JF. 2016. Cardiomyocyte specific expression of the nuclear matrix protein, CIZ1, stimulates production of mononucleated cells with an extended window of proliferation in the postnatal mouse heart. *Biology open*.

Berletch JB, Yang F, Xu J, Carrel L, Disteche CM. 2011. Genes that escape from X inactivation. *Hum Genet* **130**: 237-245.

Cobb BS, Nesterova TB, Thompson E, Hertweck A, O'Connor E, Godwin J, Wilson CB, Brockdorff N, Fisher AG, Smale ST et al. 2005. T cell lineage choice and differentiation in the absence of the RNase III enzyme Dicer. *The Journal of experimental medicine* **201**: 1367-1373.

Coverley D, Laman H, Laskey RA. 2002. Distinct roles for cyclins E and A during DNA replication complex assembly and activation. *Nature Cell Biology* **4**: 523-528.

Dobin A, Davis CA, Schlesinger F, Drenkow J, Zaleski C, Jha S, Batut P, Chaisson M, Gingeras TR. 2013. STAR: ultrafast universal RNA-seq aligner. *Bioinformatics* **29**: 15-21.

Gendrel AV, Apedaile A, Coker H, Termanis A, Zvetkova I, Godwin J, Tang YA, Huntley D, Montana G, Taylor S et al. 2012. Smchd1-dependent and -independent pathways determine developmental dynamics of CpG island methylation on the inactive X chromosome. *Dev Cell* **23**: 265-279.

Gendrel AV, Tang YA, Suzuki M, Godwin J, Nesterova TB, Greally JM, Heard E, Brockdorff N. 2013. Epigenetic functions of smchd1 repress gene clusters on the inactive X chromosome and on autosomes. *Molecular and cellular biology* **33**: 3150-3165.

Hayflick L, Moorhead PS. 1961. The serial cultivation of human diploid cell strains. *Exp Cell Res* **25**: 585-621.

Hesketh EL, Knight JR, Wilson RH, Chong JP, Coverley D. 2015. Transient association of MCM complex proteins with the nuclear matrix during initiation of mammalian DNA replication. *Cell Cycle* **14**: 333-341.

Maves KK, Weiler JM. 1992. Detection of properdin mRNA in human peripheral blood monocytes and spleen. *J Lab Clin Med* **120**: 762-766.

Moindrot B, Cerase A, Coker H, Masui O, Grijzenhout A, Pintacuda G, Schermelleh L, Nesterova TB, Brockdorff N. 2015. A Pooled shRNA Screen Identifies Rbm15, Spen, and Wtap as Factors Required for Xist RNA-Mediated Silencing. *Cell Rep* **12**: 562-572.

Mootha VK, Lindgren CM, Eriksson KF, Subramanian A, Sihag S, Lehar J, Puigserver P, Carlsson E, Ridderstrale M, Laurila E et al. 2003. PGC-1alpha-responsive genes involved in oxidative phosphorylation are coordinately downregulated in human diabetes. *Nat Genet* **34**: 267-273.

Penny GD, Kay GF, Sheardown SA, Rastan S, Brockdorff N. 1996. Requirement for Xist in X chromosome inactivation. *Nature* **379**: 131-137.

Roberts A, Trapnell C, Donaghey J, Rinn JL, Pachter L. 2011. Improving RNA-Seq expression estimates by correcting for fragment bias. *Genome Biol* **12**: R22.

Soule HD, Maloney TM, Wolman SR, Peterson WD, Jr., Brenz R, McGrath CM, Russo J, Pauley RJ, Jones RF, Brooks SC. 1990. Isolation and characterization of a spontaneously immortalized human breast epithelial cell line, MCF-10. *Cancer Res* **50**: 6075-6086.

Soule HD, Vazguez J, Long A, Albert S, Brennan M. 1973. A human cell line from a pleural effusion derived from a breast carcinoma. *J Natl Cancer Inst* **51**: 1409-1416.

Subramanian A, Tamayo P, Mootha VK, Mukherjee S, Ebert BL, Gillette MA, Paulovich A, Pomeroy SL, Golub TR, Lander ES et al. 2005. Gene set enrichment analysis: a knowledge-based approach for interpreting genome-wide expression profiles. *Proceedings of the National Academy of Sciences of the United States of America* **102**: 15545-15550.

Trapnell C, Hendrickson DG, Sauvageau M, Goff L, Rinn JL, Pachter L. 2013. Differential analysis of gene regulation at transcript resolution with RNA-seq. *Nat Biotechnol* **31**: 46-53.

Trapnell C, Williams BA, Pertea G, Mortazavi A, Kwan G, van Baren MJ, Salzberg SL, Wold BJ, Pachter L. 2010. Transcript assembly and quantification by RNA-Seq reveals unannotated transcripts and isoform switching during cell differentiation. *Nat Biotechnol* **28**: 511-515.

Wilson RH, Hesketh EL, Coverley D. 2016. Preparation of the Nuclear Matrix for Parallel Microscopy and Biochemical Analyses. *Cold Spring Harb Protoc* **2016**: pdb prot083758.

Yang F, Babak T, Shendure J, Disteche CM. 2010. Global survey of escape from X inactivation by RNA-sequencing in mouse. *Genome research* **20**: 614-622.

Yildirim E, Kirby JE, Brown DE, Mercier FE, Sadreyev RI, Scadden DT, Lee JT. 2013. Xist RNA is a potent suppressor of hematologic cancer in mice. *Cell* **152**: 727-742.

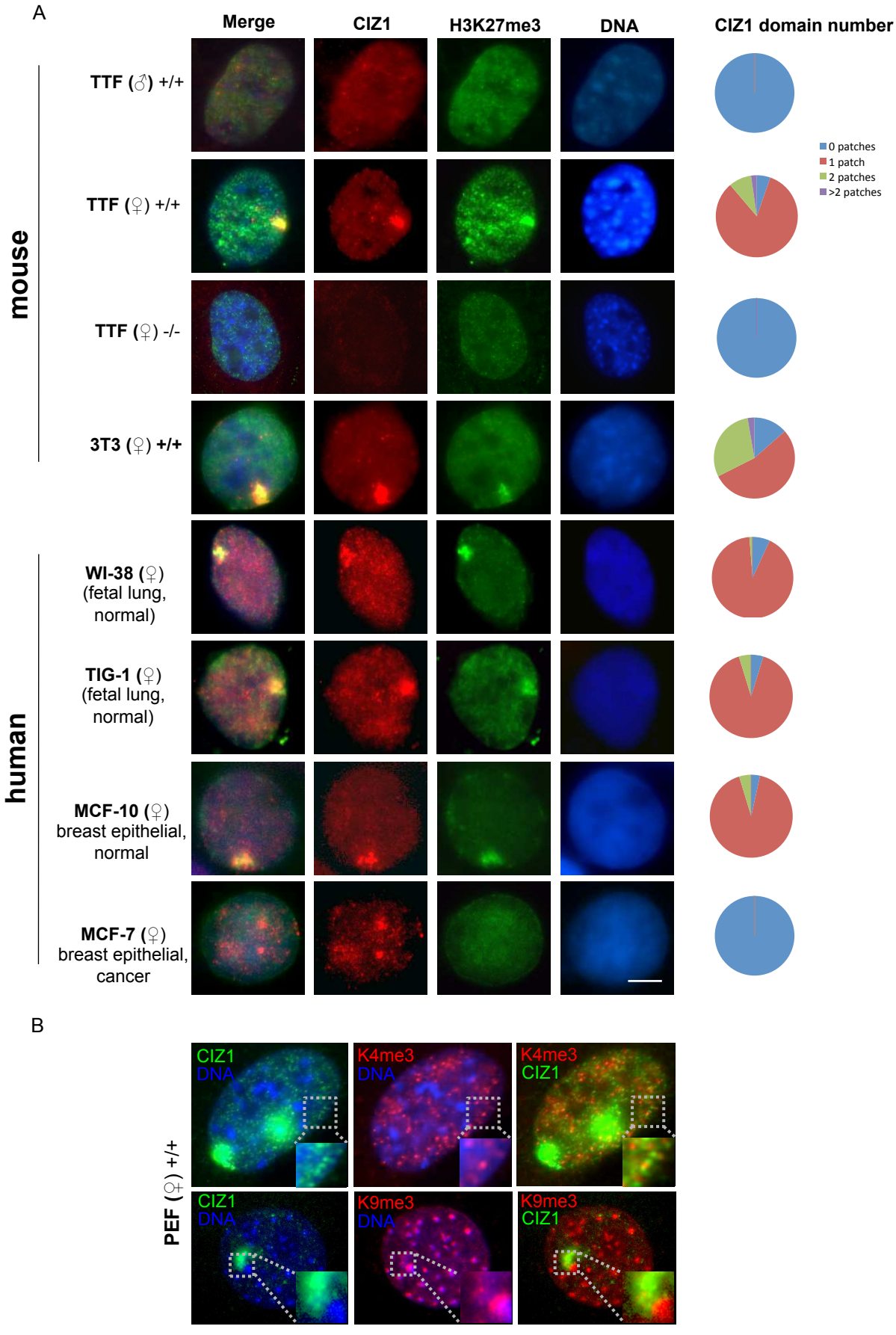
A
Merge
CIZ1
H3K27me3
DNA
CIZ1 domain number
mouse
TTF (♂) +/+
TTF (♀) +/+
TTF (♀) -/-
3T3 (♀) +/+
human
WI-38 (♀) (fetal lung, normal)
TIG-1 (♀) (fetal lung, normal)
MCF-10 (♀) breast epithelial, normal
MCF-7 (♀) breast epithelial, cancer
0 patches
1 patch
2 patches
>2 patches
B
PEF (♀) +/+
CIZ1 DNA
K4me3 DNA
K4me3 CIZ1
CIZ1 DNA
K9me3 DNA
K9me3 CIZ1

C CIZ1 expression in differentiating XX ES cells

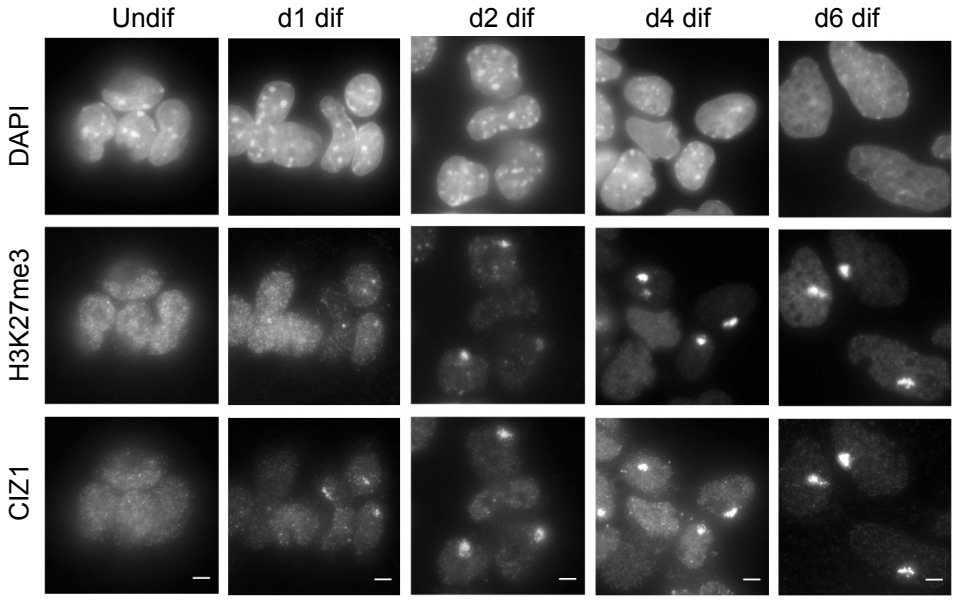

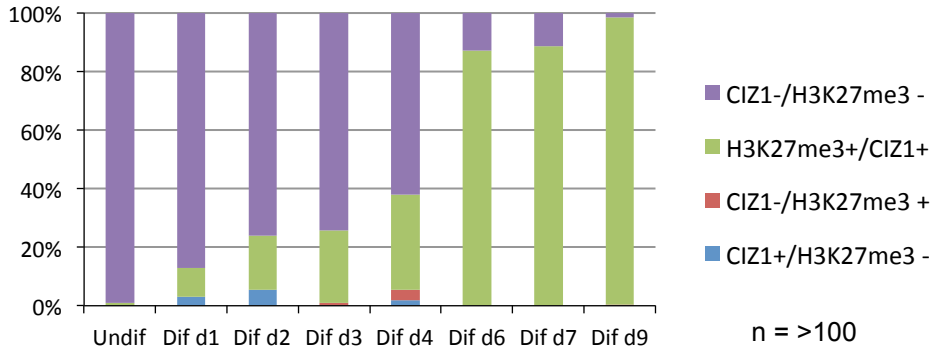

D CIZ1 during mitosis in PEFs

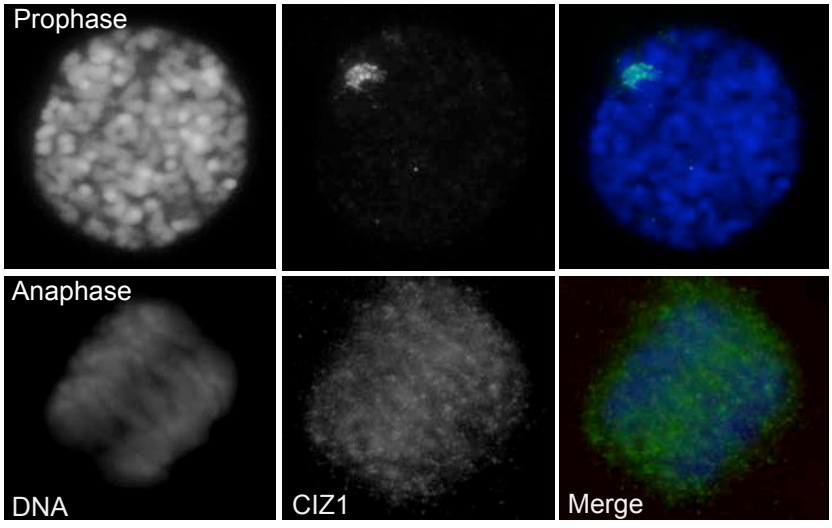

Figure S1. CIZ1 colocalizes with H3K27me3 and marks the inactive X-chromosome in multiple female cell types. Related to Figure 1. A) Representative images of mouse male, female, *Ciz1*+/+, *Ciz1*-/- cells, and human female (normal and cancer) cells as indicated, showing immunofluorescence for CIZ1-N (detected with polyclonal antibody 1794, red), H3K27me3 (green) and DNA (blue). TTF, tail-tip fibroblast. +/+ denotes wild-type, -/- denotes *Ciz1* null. Bar is 5 μm. Right, pie charts show the proportion of cells with the indicated number of CIZ1-enriched discrete domains in the nucleus (n>100). In all cases H3K27me3 domains colocalise with CIZ1 domains. CIZ1 and H3K27me3 enriched domains are not observed in male cells, though both antigens are evident throughout the nucleus. Neither are observed in female CIZ1 null cells. Notably, female MCF7 breast cancer cells exhibit an atypical pattern for both marks. B) CIZ1 (green) does not colocalise with the active chromatin marker H3K4me3 (red) or dapi-dense heterochromatin (blue), but does colocalise with a weakly marked class of H3K9me3 (red) heterochromatin distinct from that marking the dapi-dense constitutive heterochromatin. A proportion of WT primary PEFs used in this study (e13.1, e13.8 and e14.4) are tetraploid and hence have two inactive X chromosomes detected by CIZ1 antibody. C) CIZ1 recruitment to Xi closely correlates with H3K27me3 deposition during differentiation of XX ES cells. CIZ1 domains are evident from day 1 after withdrawal of LIF and become progressively stronger as differentiation proceeds. By day 9 almost 100% of cells exhibit colocalised CIZ1 and H3K27me3. D) In PEFs CIZ1 decorates Xi sister chromatids during chromosome condensation but is masked or degraded before anaphase.

A Alignment

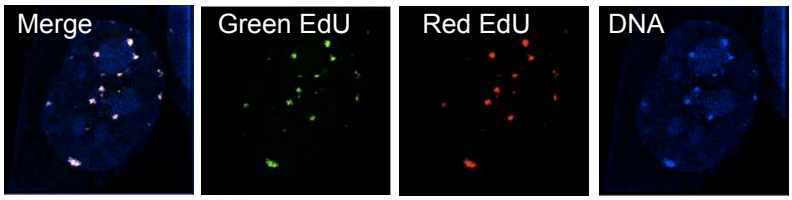

B Endogenous *Xist* in C127I somatic cells (XX)

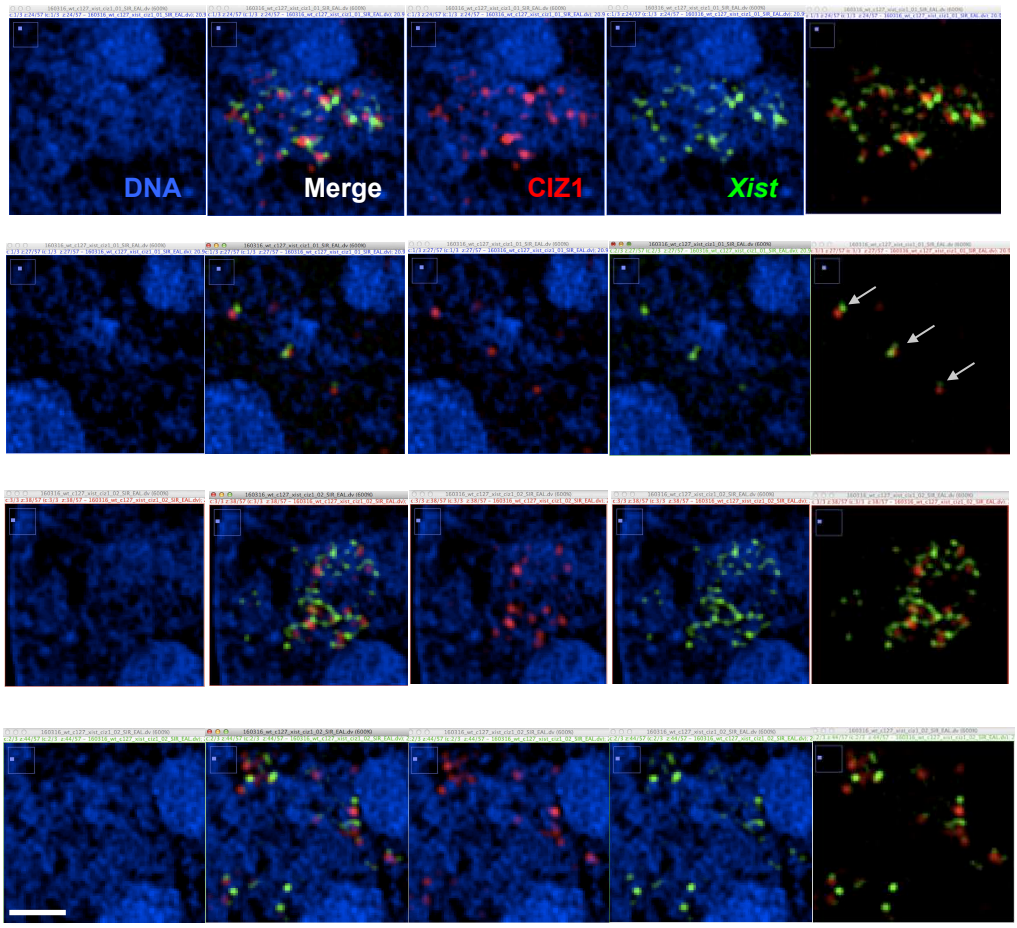

C Nuclear matrix extraction series PEFs

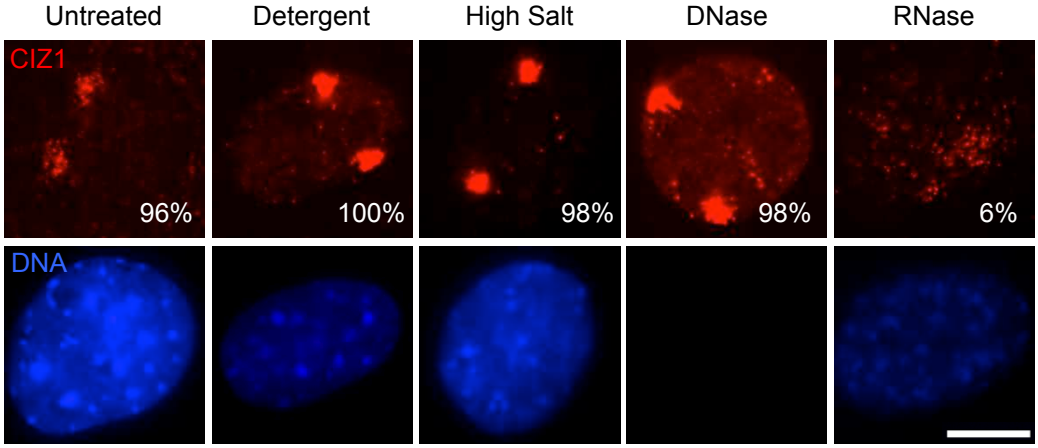

Figure S2. CIZ1 is localised adjacent to *Xist* RNA. Related to Figure 2. A) SR 3D-SIM alignment was conducted as detailed in methods and confirmed using EdU labeled C127I cells. B) Individual Z sections of the inactive X domain in XX C127I somatic cells confirms the proximal positions of CIZ1 to *Xist* RNA foci. DNA (blue), *Xist* RNA FISH (green), CIZ1 (red). Bar is 1 μm. C) Distinct populations of CIZ1 (red) revealed in female PEFs by serial NM extraction as shown for 3T3 cells in main Figure 2. The proportion of cells with discrete CIZ1-Xi domains is indicated (n>50 for each extraction condition). A proportion of WT primary PEFs (e13.1, e13.8 and e14.4) are tetraploid and contain two CIZ1 domains as shown. All images are captured and shown under identical conditions. DNA (blue) shows the extent of nuclease treatment. Bar is 5 μm.

A YY1 in 3T3 cells

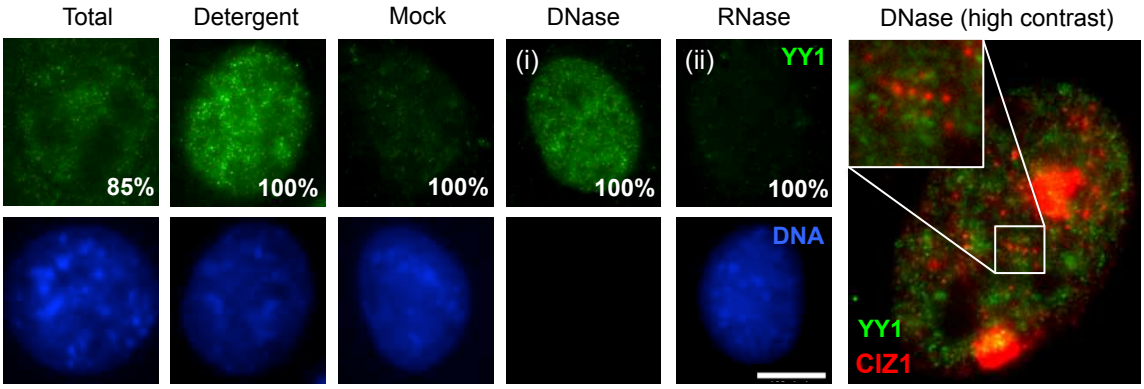

B SAF-A in 3T3 cells

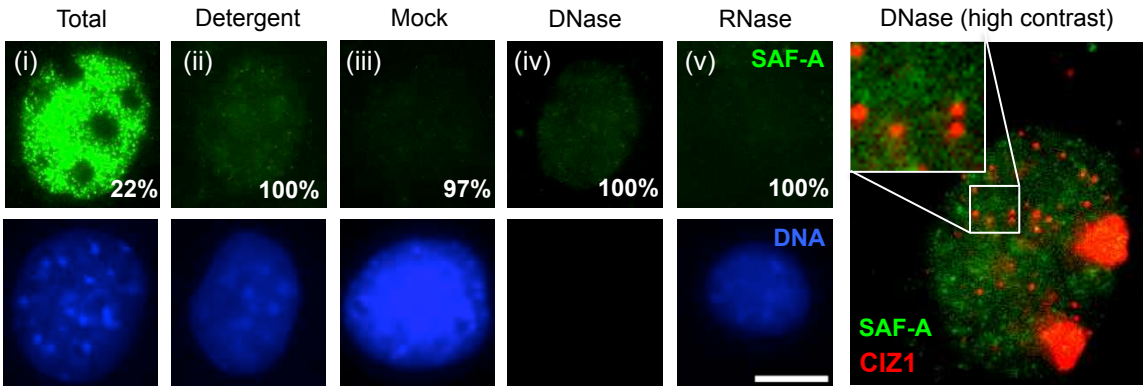

Higher intensity SAF-A images showing increased staining after removal of chromatin

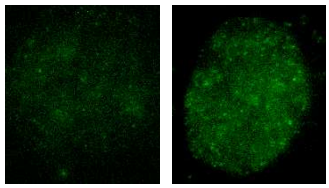

C SAF-A in 3T3 cells

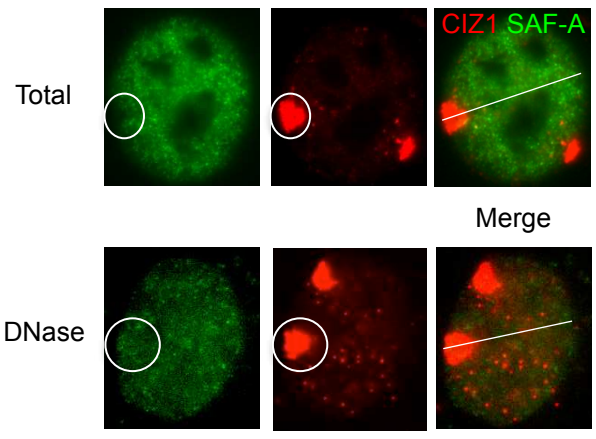

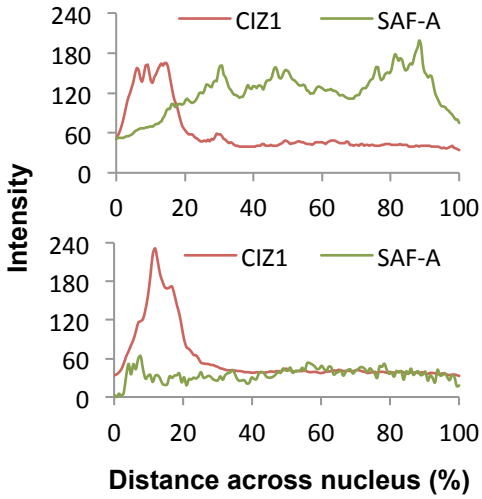

Figure S3. Nuclear matrix proteins implicated in X chromosome inactivation. Related to Figure 2. Examples of tetraploid cells with two CIZ1 domains are shown, which represent ~30% of the cells in this line (3T3). A) Immuno-detection of YY1 after serial extraction with the indicated treatments showing (i) retention after removal of chromatin, but (ii) loss after removal of RNA in female 3T3 cells. All cells in the cycling population behaved similarly. Right, NM-associated YY1 does not colocalise with CIZ1 (detected with 1794) at Xi or elsewhere in the nucleus. B) Immuno-detection of SAF-A after serial extraction with the indicated treatments, showing (i) a mixed staining population in which ~25% have high levels of SAF-A (shown), (ii) loss of the bright staining population after treatment with detergent indicating lack of association of this population with the NM, (iii) further reduction of staining after incubation in high-salt buffer (mock), and (iv) a boost in signal when chromatin is removed indicating masked epitope (also for YY1). (v) Complete extraction of SAF-A when RNA is removed, indicating that the insoluble SAF-A fraction is immobilized by attachment to the RNA-dependent NM. Right, NM-associated SAF-A does not colocalise with CIZ1. In all cases staining, image capture and manipulation parameters were constant, so that image intensities within a series reflect actual relationships. A higher-intensity pair of images for SAF-A is also shown. C) After extraction of chromatin to reveal buried epitope SAF-A is detected in the Xi territory, defined by co-staining for CIZ1. Lines in merged images show section quantified in graphs, right, using NIH image J (arbitrary units). Images of total and DNase treated nucleus are enhanced differently to reveal position rather than relative intensity.

A *Xist* transgene in undifferentiated male (XY) ESCs

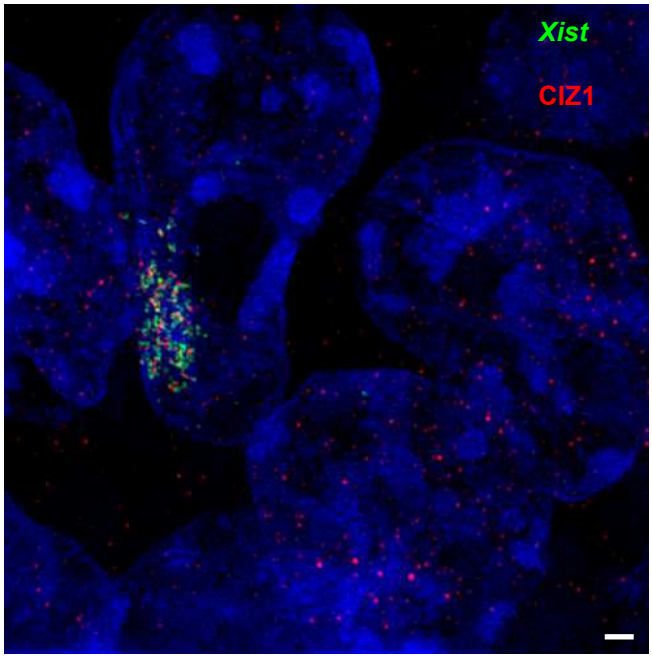

B CIZ1 localisation in *Xist* mutant MEF lines

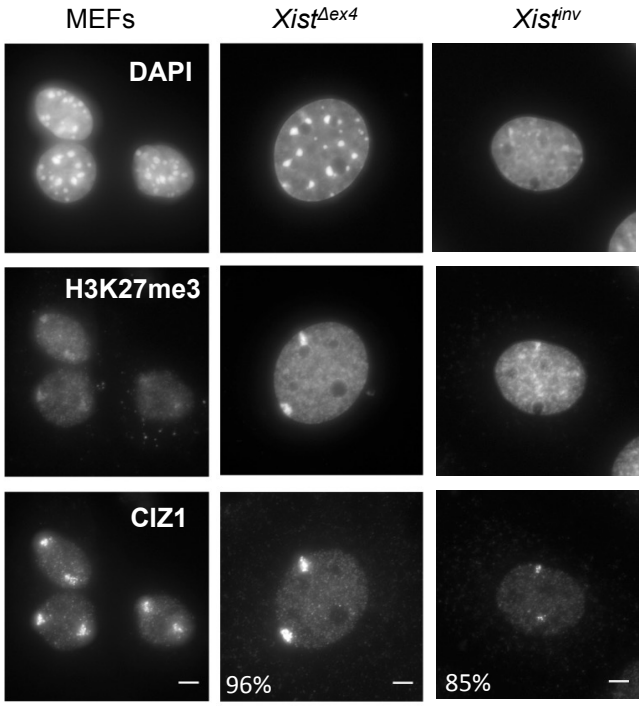

Figure S4 Related to Figure 3. A) SR 3D-SIM of induced *Xist* transgene in XY MG-3E ES cells, showing recruitment of CIZ1 (red) upon induction of full length *Xist* (green). Bar=1 μm. B) CIZ1 localisation in *Xist* mutants. $Xist^{\Delta ex4}$ is a deletion of conserved exon 4 (Caparros et al. 2002). 96/100 cells exhibited colocalisation of CIZ1 and H3K27me3, with 4/100 showing neither mark. $Xist^{inv}$ is a hypomorphic allele containing an inversion of 7kb of *Xist* genomic sequence spanning from the middle of repeat D to exon 5. Exon 4 is also missing in this mutant (Senner et al. 2011). 85/100 cells showed CIZ1 and H3K27me3 colocalisation, 11/100 showed neither mark, and 4/100 were positive for CIZ1 only.

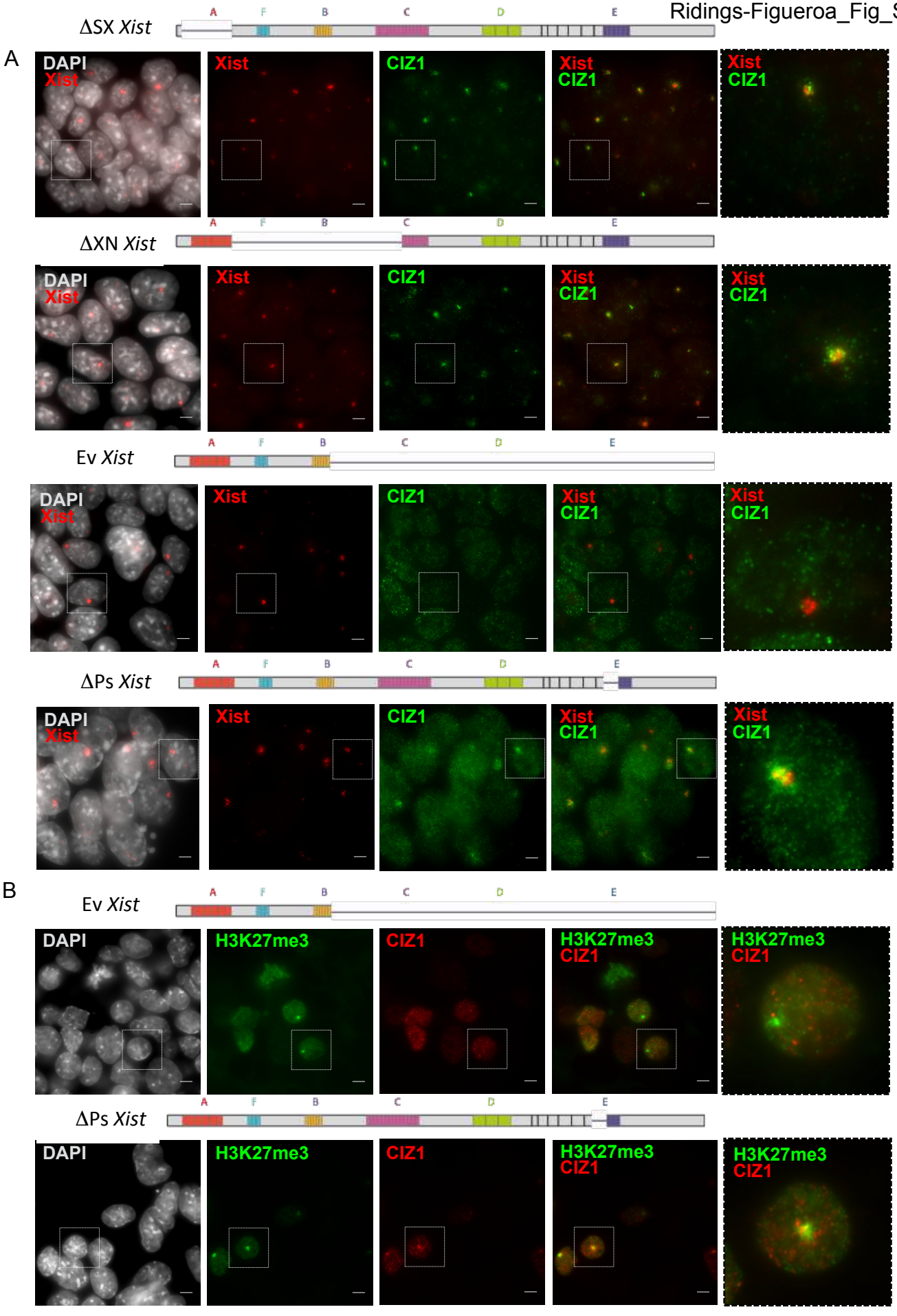
A
ΔSX Xist
A F B C D E
DAPI
Xist
Xist
CIZ1
Xist
CIZ1
Xist
CIZ1
ΔXN Xist
A F B C D E
DAPI
Xist
Xist
CIZ1
Xist
CIZ1
Xist
CIZ1
Ev Xist
A F B C D E
DAPI
Xist
Xist
CIZ1
Xist
CIZ1
Xist
CIZ1
ΔPs Xist
A F B C D E
DAPI
Xist
Xist
CIZ1
Xist
CIZ1
Xist
CIZ1
B
Ev Xist
A F B C D E
DAPI
H3K27me3
CIZ1
H3K27me3
CIZ1
H3K27me3
CIZ1
ΔPs Xist
A F B C D E
DAPI
H3K27me3
CIZ1
H3K27me3
CIZ1
H3K27me3
CIZ1

Figure S5 Recruitment of CIZ1 by *Xist* transgenes in male (XY) P4D7 ES cells. Related to Figure 3. A) Immuno-FISH for *Xist* (red) and CIZ1 (green, N-term) in ES cells. B) H3K27me3 (green) and CIZ1 (red) in ES cells. Ev *Xist* localizes to Xi and supports H3K27me3 at Xi, but does not recruit CIZ1.

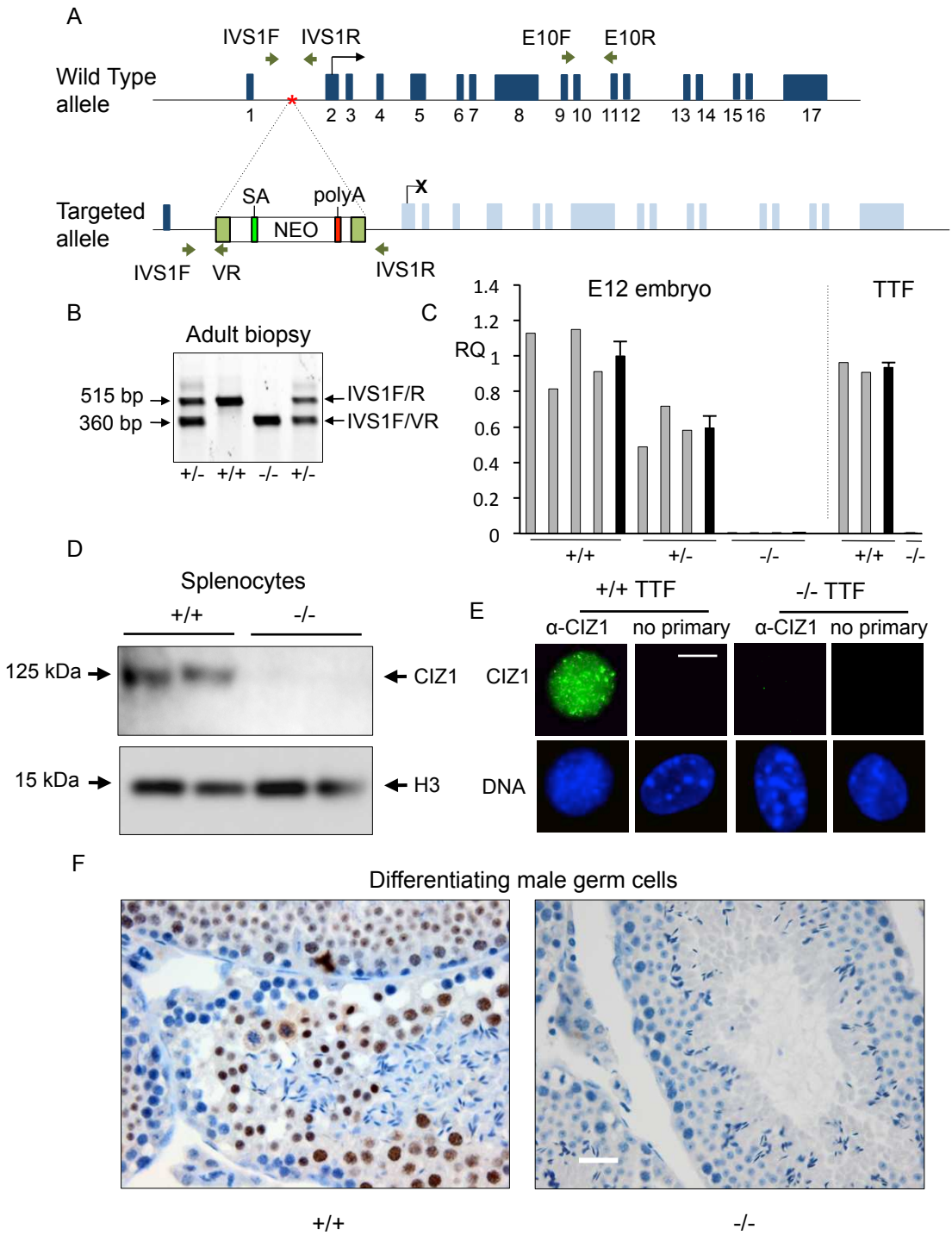
A
IVS1F
IVS1R
E10F
E10R
Wild Type allele
1
2 3
4
5
6 7
8
9 10
11 12
13 14 15 16
17
Targeted allele
SA
polyA
NEO
X
IVS1F
VR
IVS1R
B
Adult biopsy
515 bp
360 bp
IVS1F/R
IVS1F/VR
+/- +/+ -/- +/-
C
E12 embryo
TTF
RQ
1.4
1.2
1
0.8
0.6
0.4
0.2
0
+/+ +/- -/- +/+ -/-
D
Splenocytes
+/+
-/-
125 kDa
CIZ1
15 kDa
H3
E
+/+ TTF
-/- TTF
α-CIZ1
no primary
α-CIZ1
no primary
CIZ1
DNA
F
Differentiating male germ cells
+/+
-/-

Figure S6 Generation and validation of *Ciz1* null (-/-) mice and derived cell populations. Related to Figure 5. A) Schematic of gene trap insertion strategy, with selection cassette in intron 1 of *Ciz1* in the C57BL/6 genome. Location of primers used for genotyping (IVS1F, IVS1R, VR) and expression analysis (E10F, E10R) are indicated. Dark blue boxes are expressed exons. Pale blue boxes are exons that are not expressed following cassette insertion. NEO; neomycin resistance gene, SA; splice acceptor site, polyA; polyadenylation signal. B) Genotyping strategy using primers IVS1F, IVS1R and VR on DNA isolated from ear biopsy to detect wild type allele (515 bp) and targeted allele (360 bp). C). Quantitative RT-PCR showing mRNA expression in *Ciz1*+/+, +/- and -/- embryos from 2 litters (left), at day 12 of gestation, and (right) from tail tip fibroblasts (TTFs) at passage 3, derived from *Ciz1*+/+ and *Ciz1*-/- mice, all detected with E10F and E10R. Results are normalised to *GapdH,* then calibrated to a mean *Ciz1*+/+ value of 1.0. Grey bars show individual data, black bars are mean result for each genotype, ±SEM. D). Western blot of splenocyte total cell lysate probed with CIZ1-N antibody 1794. Histone H3 is shown as loading control. E). Representative immunofluorescence of total CIZ1 protein in *Ciz1*+/+ and *Ciz1*-/- TTFs, detected via CIZ1-N antibody 1793. DNA is counterstained with Hoechst 33258, bar is 10 μm. F). Representative immunohistochemical analysis of CIZ1 (brown) in testis (where expression is normally highest (Greaves et al. 2012)), detected with CIZ1-N antibody 1793. Cells are counter-stained with Haematoxylin (blue). Bar is 50μm.

A

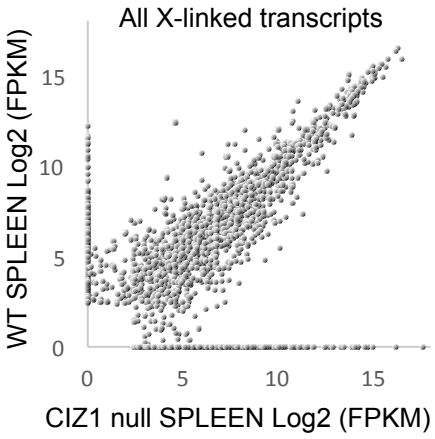

B

	X-chromosome	Whole-genome
Fold change	% changed	% changed
-2	8.73	16.8
-1.5	12.9	20.2
1.5	20.5	21.6
2	16.4	17.9

D

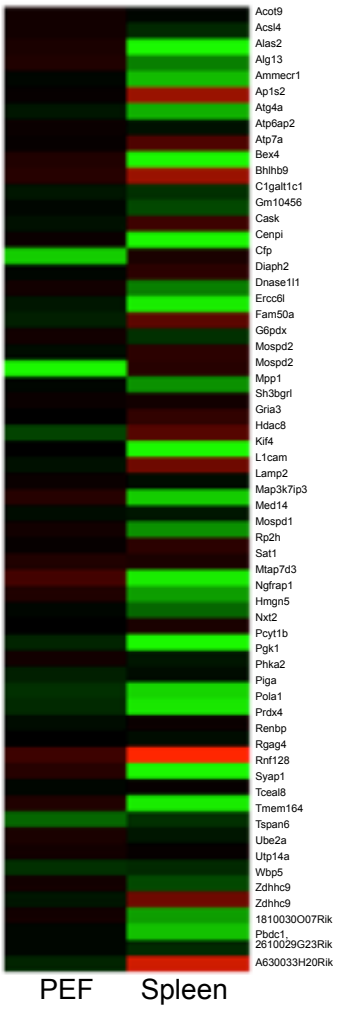

C

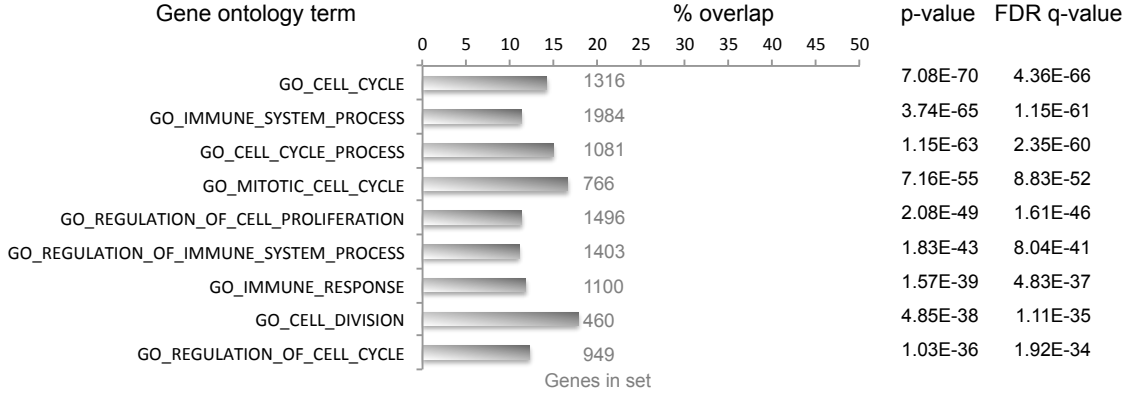

Figure S7. Analysis of gene expression in spleen. Related to Figure 7. A) Expression of all X-linked transcripts in WT and CIZ1 null spleen (FPKM). B) Summary of the proportion of genes up and down regulated at the indicated thresholds. C) Gene set enrichment analysis (Subramanian et al, 2005) showing representation of genes that are more than 2-fold changed in CIZ1 null spleen (up or down) among the indicated gene ontology terms, and immunological signatures, with significance indicators. D) X-linked transcripts that are de-repressed upon loss of *Xist*, identified by Yildrim et al (2013) and also changed in response to loss of CIZ1. Status in CIZ1 KO spleen and PEFs are shown relative to WT.